Size-dependent effects of the thermal transport at gold nanoparticle–water interfaces

Oscar Gutiérrez-Varela, Samy Merabia, Ruben Santamaria

Size-dependent effects of the thermal transport at gold nanoparticle-water interfaces

Article *in* The Journal of Chemical Physics · July 2022

DOI: 10.1063/5.0096033

3 authors:

Oscar Gutiérrez-Varela
Universidad Nacional Autónoma de México
6 PUBLICATIONS **10** CITATIONS
SEE PROFILE

Samy Merabia
French National Centre for Scientific Research
113 PUBLICATIONS **2,516** CITATIONS
SEE PROFILE

Ruben Santamaria
Universidad Nacional Autónoma de México
52 PUBLICATIONS **633** CITATIONS
SEE PROFILE

Size-dependent effects of the thermal transport at gold nanoparticle-water interfaces

Oscar Gutiérrez-Varela

Instituto de Física, Universidad Nacional Autónoma de México, Ciudad de México, México and

Univ. Lyon, Université Claude Bernard Lyon 1, CNRS,

Institut Lumière Matière, F-69622, Villeurbanne, France

Samy Merabia[a]

Univ. Lyon, Université Claude Bernard Lyon 1, CNRS,

Institut Lumière Matière, F-69622, Villeurbanne, France

Ruben Santamaria

Instituto de Física, Universidad Nacional Autónoma de México, Ciudad de México, México

(Dated: July 14, 2022)

Abstract

The transfer of heat from a plasmonic nanoparticle to its water environment has numerous applications in the fields of solar energy conversion and photothermal therapies. Here, we use non-equilibrium molecular dynamics to investigate the size-dependent effects of the interfacial thermal conductance of gold nanoparticles immersed in water and with tunable wettability. The interfacial thermal conductance is found to increase when the nanoparticle size decreases. We rationalize such a behavior with a generalized acoustic model, where the interfacial bonding decreases with the nanoparticle size. The analysis of the interfacial thermal spectrum reveals the importance of the low frequency peak of the nanoparticle spectrum as it matches relatively well the oxygen peak in the vibrational spectrum. However, by reducing the nanoparticle size, the low frequency peak is exacerbated, explaining the enhanced heat transfer observed for small nanoparticles. Finally, we assess the accuracy of the continuum heat transfer equations to describe the thermal relaxation of small nanoparticles with initial high temperatures. We show that, before the nanoparticle looses its integrity, the continuum model succeeds in describing with small percentage deviations the molecular-dynamics data. This work brings a simple methodology to understand, beyond the plasmonic nanoparticles, thermal boundary conductance between a nanopartice and its environment.

[a] Corresponding author: samy.merabia@univ-lyon1.fr

I. INTRODUCTION

Understanding the way in which heat is transferred from a metallic nanoparticle to the surrounding liquid is of great interest for numerous technological applications. This explains the increased interest in the last two decades in the thermophysical properties of metallic nanoparticles dispersed in a liquid environment. Potential applications encompass thermal management of liquids, mass transport [1, 2], drug delivery [3], oil recovery [4], pollutant reduction in buildings [5], solar energy conversion [6], among other important topics [4, 7, 8].

A fundamental understanding of thermal transport at the nanoscale presents significant experimental challenges due to both, the small spatial dimensions and the short time scales relevant to the nanoparticles. These challenges have been addressed by different groups by employing time-resolved optical techniques, where the colloidal nanoparticles are initially heated up by a short-pulse laser. The nanoparticle temperature kinetics may be followed by either pump-probe time-resolved reflectance or X-ray scattering, which can give evidence of the loss of the nanoparticle crystallinity due to the laser heating [9], also demonstrating the possible phase explosion, and the subsequent generation of plasmonic nanobubbles after the excitation with a high intensity laser [10]. Under moderate excitation, it is found that the heat transfer from the nanoparticle to its water environment is well described by the continuous heat transfer equations, supplemented with a finite thermal interfacial conductance, G_k [9]. The typical values of G_k are in the range $10 - 300$ MW $\cdot$ m^{-2} K^{-1}, and depend of several characteristics, including the nature of the nanoparticles [11], their shapes [12], the presence of surfactants [12, 13], their wetting properties [14], and the chemical nature of the solvent [11, 15] as well.

Concurrently, thermal transport around hot colloidal nanoparticles has been modeled using molecular dynamics (MD) simulations. The early studies were concentrated on small nanoparticles dispersed in water [16, 17, 19], while more recent works have considered extreme heating conditions [20, 21]. The thermal conductance at the interface between the gold nanoparticle and water has been shown to depend on the interface wetting properties [22]. The nanoparticle curvature is a parameter which also plays an important role in interfacial heat transport [23–25]. Different qualitative results have been obtained so far: for gold nanoparticles immersed in a Lennard-Jones fluid, the conductance is found to increase with the nanoparticle curvature [24], while the opposite behavior is observed for gold nanoparticles in toluene [23]. The size-dependence of the interfacial heat transfer process has been characterized beyond the colloidal nanoparticle systems, and has included nanocrystal arrays at the organic-inorganic interface

[26], octane droplets in water [27], and bubbles [28]. The size-dependent effects of the thermal conductance $G_k(R_{np})$ are generally described with an empirical relation, $G_k(R_{\rm np}) = G_0 + \delta/R_{\rm np}$ [24], where $R_{\rm np}$ is the nanoparticle radius and δ is a characteristic length on the order of a molecular size.

Characterizing the size-dependent transport properties of the metallic nanoparticle is critical to accurately understand thermal transport in colloidal gold nanoclusters. Gold nanoclusters have diameters smaller than 2 nm, and corresponding number of atoms typically less than 100. Presently, it is possible to experimentally synthesize metal nanoparticles with diameters down to 1 nm [29, 30]. On the other side, the simulations of gold nanoclusters in water under realistic conditions are scarce in the literature, with the exception of a few studies [16, 17]. These studies do not address the size-dependent effects of the interfacial thermal transport. Another question that we address here concerns the accuracy of continuum models to describe heat transfer around very small (down to $R_{\rm np} = 0.5$ nm) nanoclusters in water. Experiments show that continuum elasticity is valid for surprisingly small nanoparticles, $R_{\rm np} = 0.5$ nm [18]. Less is known regarding heat transfer at such small length scales and under strongly out of equilibrium conditions.

In this work we investigate how the thermal interface conductance depends on the nanoparticle size, and assess the predictions of the continuum model on the heat transfer of small nanobjects. To do this, we analyze in detail the thermal transport of spherical gold nanoparticles, with diameters ranging from 1 up to 8 nm, immersed in water by employing non-equilibrium molecular dynamics simulations. It is shown that the interfacial thermal conductance increases by reducing the nanoparticle size. We rationalize the size-dependent effects with a generalized acoustic model, where the interfacial bonding increases with the nanoparticle curvature. A thermal spectrum analysis allows us to determine the vibrational modes with major contributions to the interfacial heat transfer, and explore the vibrational coupling changes of the gold nanocluster-water interface with the nanoparticle size. Finally, we consider the description of a continuum model of the heat transfer process between the heated nanoparticle and surrounding water.

The paper is structured as follows. Section II describes the analytical acoustic model, the molecular system, and the methodology of this work. Section III presents the main results: first, the behavior of the thermal conductance at the interface of the nanoparticle-water bulk environment, and in terms of the nanoparticle size, is shown. Here, we interpret the dependence

of the interfacial thermal conductance by employing different physical quantities such as the potential energy at the interface, the density of vibrational states and the frequency-dependent heat flux. Finally, a continuum model is evaluated and its accuracy assessed with respect to the thermal relaxation of small nanoparticles with initial high temperatures. Section IV provides the main results on the behavior of the interfacial thermal conductance of small nanoparticles, like the reduction of the interfacial potential energy and the exacerbation of the low vibrational frequencies as the nanoparticles become smaller.

II. ACOUSTIC MODEL AND SIMULATION METHODOLOGY

This section briefly describes both, the acoustic model which is proposed to understand the thermal conductance in terms of the cluster size and the molecular dynamics methodology.

A. Acoustic model for the size-dependent conductance

The purpose of this section is to present a simple analytical model to predict the size-dependent thermal conductance at the interface of the nanoparticle and water. To this end, we employ a recent generalized acoustic mismatch model designed to tackle heat transport at the solid-liquid interface [31].

The thermal conductance is given by:

$$G_k = \sum_p \int_0^{\omega_{\max}} k_B g_p(\omega) v_p(\omega) \tau_p(\omega) d\omega \tag{1}$$

p is an index denoting the transverse and longitudinal polarization, $\omega_{\max}$ is the maximal frequency of the vibrational spectrum of the nanoparticle, $g_p(\omega)$ is the nanoparticle vibrational density of states, $v_p(\omega)$ the corresponding group velocity, and $\tau_p(\omega)$ is the phonon transmission function. It is convenient to adopt an acoustic model of τ_p given in [31, 32], which approximately explains the heat transfer at the interface of two media:

$$\tau_p(\omega) = \frac{Z_{\rm np}(\omega) Z_{\rm wat}(\omega)}{(Z_{\rm np}(\omega) + Z_{\rm wat}(\omega))^2 + \frac{\omega^2}{K^2(R_{\rm np})} (Z_{\rm np}(\omega) Z_{\rm wat}(\omega))^2} \tag{2}$$

$Z_{\rm np}(\omega)$ and $Z_{\rm wat}(\omega)$ are the acoustic impedance of the nanoparticle and water, respectively (we omitted the polarization index for simplicity).

We assume a harmonic interaction between the nanoparticle atoms and the water atoms with a spring stiffness given by $K(R_{\rm np})$ [31, 32]. The spring stiffness may be written as the

product of the interface potential curvature $\frac{d^2V}{dr^2}$ and the number of gold-water contacts per surface unit, $\sigma(R_{\rm np})$. To estimate how this latter quantity depends on the nanoparticle radius $R_{\rm np}$, we adopt a simple model proposed by Jimenez et al. [33]. Let us consider a water molecule interacting with the gold nanoparticle as represented in Fig. 1. We assume a simple model

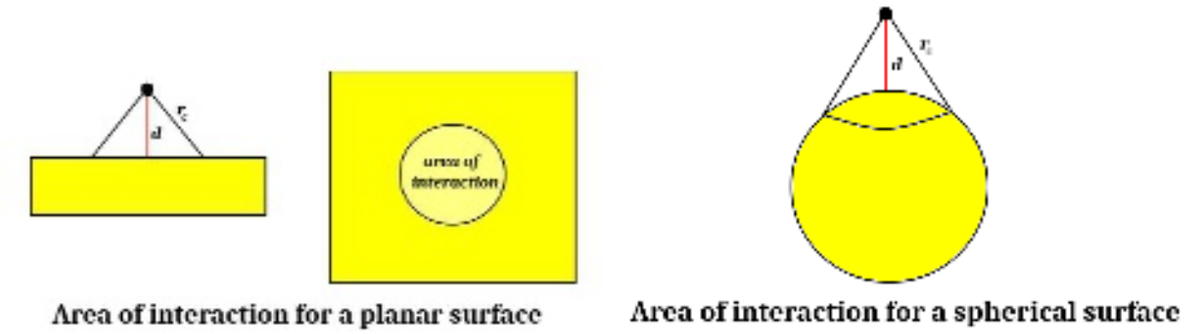

(a) (b)

FIG. 1: Illustration of the curvature dependent area of interaction at the water-gold interface. a): planar interface. b): curved interface. These illustrations are inspired by [33].

where a water molecule interacts with a gold atom if their distance d is smaller than a cut-off radius r_c. Below this cut-off the interaction is supposed to be constant, independent on the distance d. We now give the expression of the area of interaction $s_{\rm R_{np}}(d)$, defined as the area of gold atoms interacting with a water molecule at a distance d from the interface. First, for a planar interface, it can be prove that:

$$s_{R_{\rm np}\to\infty}(d) = \pi(r_c^2 - d^2) \tag{3}$$

For a curved interface, the area of interaction is increased with respect to the planar case:

$$s_{R_{\rm np}}(d) = \pi\frac{(r_c^2 - d^2)}{(1 + d/R_{\rm np})} \tag{4}$$

From these two equations, we conclude that the surface density of gold-water contacts $\sigma(R_{\rm np})$ may be written as:

$$\sigma(R_{\rm np}) = 1/s_{R_{\rm np}}(\delta) = \sigma(\mathrm{R_{np}} \to \infty)\,(1 + \delta/\mathrm{R_{np}}) \tag{5}$$

$\sigma(\mathrm{R_{np}} \to \infty) = 1/(\pi(\mathrm{r_c^2} - \delta^2))$ is the surface density corresponding to a flat interface, and we denoted with δ the average interaction distance between a gold atom and a water molecule. From such considerations, we deduce that $K_{R_{\rm np}}$ may be expressed as:

$$K(R_{\rm np}) = K(\mathrm{R_{np}} \to \infty)\,(1 + \delta/R_{\rm np}) \tag{6}$$

with obvious notations.

In the limit where the binding stiffness is weak, one has the approximation:

$$(Z_{\rm np}(\omega)+Z_{\rm wat}(\omega))^2+\frac{\omega^2}{K^2(R)}(Z_{\rm np}(\omega)Z_{\rm wat}(\omega))^2\simeq\frac{\omega^2}{K^2(R_{\rm np})}(Z_{\rm np}(\omega)Z_{\rm wat}(\omega))^2$$

$$\tau_p(\omega)\simeq K^2(R_{\rm np})/\omega^2\propto(1/\omega^2)(1+\delta/R_{\rm np})^2 \tag{7}$$

After taking these considerations in Eq. 1, the resulting interfacial thermal conductance is:

$$G_k(R_{\rm np})\simeq G_k(\infty)\left(1+\frac{\delta}{R_{\rm np}}\right)^2 \tag{8}$$

$G_k(\infty)$ is the conductance of the corresponding flat interface. Alternatively, we will compare the MD simulation data to the empirical relation proposed in [24]:

$$G_k(R_{np})=G_K(\infty)\left(1+\frac{\delta}{R_{np}}\right) \tag{9}$$

B. Atomic and molecular structure

The system consists of a gold nanoparticle immersed in water. Water is described by the TIP4P/2005-water model, with flexible covalent bonds OH and bond angles H-O-H. The covalent bonds and bond angles are simulated using harmonic potentials, whose equilibrium parameters are $r_0 = 0.9572$ Å, $k_r = 600.0$ Kcal/(mol Å^2), $\theta_0 = 104.52^o$ and $k_\theta = 75.0$ Kcal/(mol rad Å). The Lennard-Jones (LJ) 12-6 potential, with equilibrium parameters $\sigma_{OO} = 3.1589$ Å and $\epsilon_{OO} = 0.1852$ Kcal/mol [34] for the non-bonded interactions between oxygen atoms were also considered. In addition to the LJ non-bonded interactions, the water molecules interact using the Coulomb potential. The atomic charges are $q_O = 0$, $q_M = -1.1128e$, and $q_H = 0.5564e$ for oxygen, M-site, and hydrogen, respectively.

A gold nanoparticle with initial FCC-type crystalline structure and occupying $\sim 1\%$ of the total box volume, is constructed. The interactions among the gold atoms of the nanoparticle are described by the 12-6 Lennard-Jones potential, with parameters $\sigma_{AuAu} = 2.6290$ Å and $\epsilon_{AuAu} = 5.29$ Kcal/mol [35]. The interaction between the nanoparticle atoms and the water molecules is modeled by a 12-6 LJ potential, with parameters $\sigma_{NpO} = \sigma_{AuO} = 2.8818$ Å and $\epsilon_{NpO} = \alpha\epsilon_{AuO}$, $\epsilon_{AuO} = 0.9898$ Kcal/mol. The dimensionless parameter α is introduced to change the wetting properties of the nanoparticle. This parameter modifies the interaction between the nanoparticle and the water oxygens and, in turn, modifies the contact angle between the nanoparticle and the water atoms (the contact angle is that one formed by the surface

of the liquid in contact with the solid). Both parameters σ_{AuO} and ϵ_{AuO} are given by the geometric-mean combination rule $\sigma_{ij} = (\sigma_{ii}\sigma_{jj})^{1/2}$ and $\epsilon_{ij} = (\epsilon_{ii}\epsilon_{jj})^{1/2}$. All the interactions are truncated at 11 Å, and the Coulomb interactions beyond this cut-off are calculated using the Ewald summation.

The nanoparticle wetting properties are tuned by changing the value of α to describe: i) a strongly wetting nanoparticle with $\alpha = 1.0$, corresponding to a contact angle of 19^o, ii) the intermediate wetting nanoparticle with $\alpha = 0.5$, giving a contact angle of 39^o, and iii) a weakly wetting nanoparticle with $\alpha = 0.3$, leading to a contact angle of 71^o. The values of the contact angles were determined in separate simulations, where a water drop was allowed to relax its shape on a flat gold surface. In the following, we consider different nanoparticle diameters, going from 1 nm to 8 nm.

C. MD methodology, data collection and analysis

The time step used in all the simulations is 1 fs. In a first stage, all the simulated systems are thermally equilibrated in the NPT ensemble, with $P = 1$ atm and $T = 300$ K. The Nose-Hoover barostat-thermostat approach is used. In a later stage, the same temperature is employed in the NVT ensemble. To do this, a heat sink was employed. It has spherical geometry, and a volume that occupies approximately 1/10 of the simulation box. The water molecules in the heat-sink region are thermalized to $T = 300$ K (Fig. 2). With the purpose to prevent the displacement of the nanoparticle due to its Brownian motion, a spring force with constant $k_s = 100.0$ Kcal/(mol Å^2) is applied to each atom of the nanoparticle. Once the thermal equilibrium is achieved, two types of simulations are unfolded: simulations with a steady heat flux, and simulations with a transient cooling. The details of how the data are collected are explained in the supplementary material (SM).

D. Measurement of interfacial thermal conductance

In order to determine the interfacial thermal conductance, we consider transient simulations. The nanoparticle is first heated up to 500 K for 40 ps. Later, it is allowed to cool down as previously described, and we register the nanoparticle temperature every 25 ps. At the same time, the water bulk temperature is fixed at 300 K using the Nose-Hoover thermostat. The nanoparticle temperature, $T_{\rm np}$, in the cooling process as determined from the MD simulations

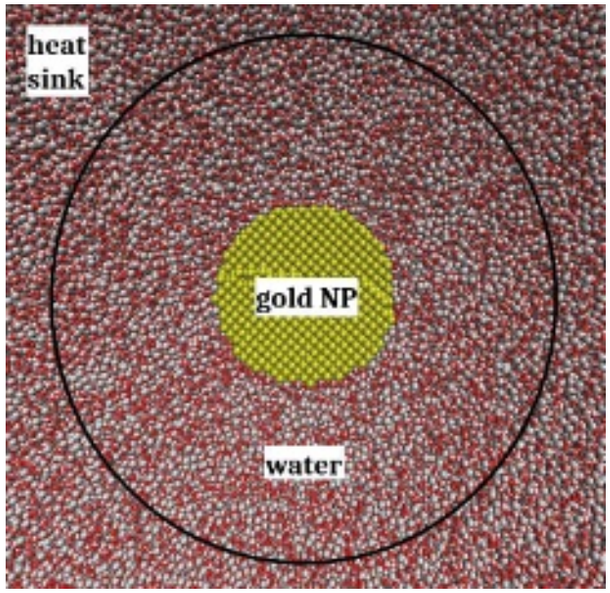

FIG. 2: Illustration of the system: a gold nanoparticle surrounded by liquid water. The big black circle delimits the location of the heat sink.

is employed to determine the interfacial thermal conductance, G_k, from the Eq. below:

$$C_p \frac{dT_{\rm np}(t)}{dt} = -A_{\rm np} G_k \left(T_{\rm np}(t) - T_s\right), \tag{10}$$

C_p is the nanoparticle heat capacity, $A_{np} = 4\pi R_{\rm np}^2$ the area of the nanoparticle, and T_s the water surface temperature. The general solution of Eq. 10 gives the nanoparticle temperature with time, $T_{np}(t) = C_1 e^{-C_2 t} + C_3$. The coefficients C_1, C_2, and C_3 are fitted from the MD simulation data. Thereby, we calculate G_k from $C_2 = A_{np} G_k / C_p$, which is obtained by substituting $T_{np}(t)$ in Eq. 10.

III. RESULTS AND DISCUSSION

A. Size-dependent conductance

1. Thermal conductance from MD simulations

The conductance of gold nanoparticles as a function of their radius for the three wetting regimes -strongly wetting, intermediate, and weakly wetting- is illustrated in Fig. 3a. For all the types of nanoparticles, the conductance increases when the nanoparticle size decreases. Fig. 3a shows that both functional forms, the quadratic function of the acoustic model, Eq. (8), and the empirical formula proposed in [24], Eq. (9), provide a good description of the size effects of the nanoparticle-water interfacial thermal conductance. The values of the parameters $G_K(\infty)$

and δ are given in Table I. The value of the infinite radius thermal conductance, $G_K(\infty)$, ranges from 49 MW/(K $\cdot$ m^2) for weakly wetting interfaces to 143 MW/(K $\cdot$ m^2) for strongly wetting interfaces.

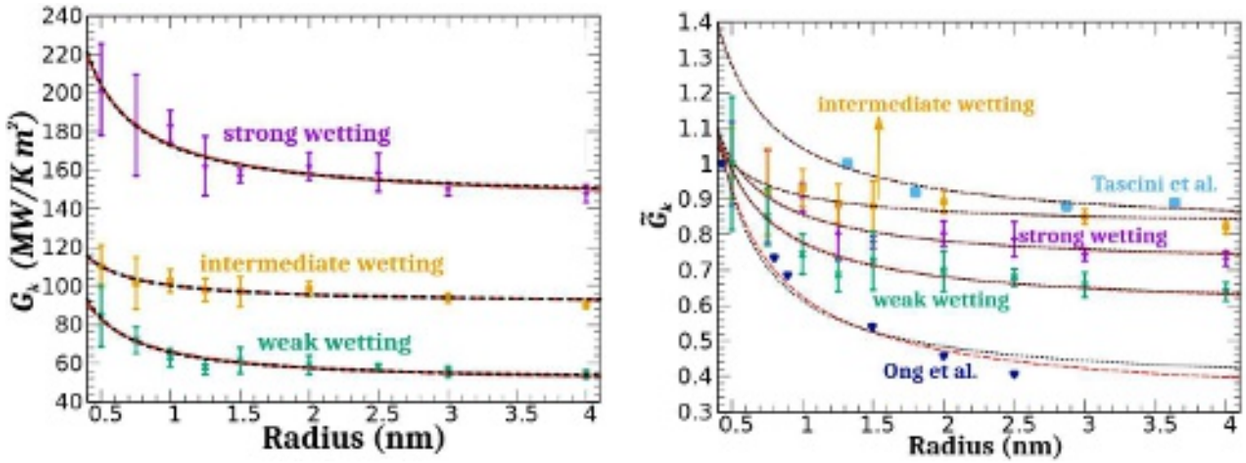

(a) (b)

FIG. 3: a) Gold-water thermal interface conductance, G_k, as a function of the gold nanoparticle radius for the different wettings. The values of the length δ and the conductance $G_K(\infty)$ are given in Table I. b) Normalized interfacial conductance in terms of the nanoparticle radius. The MD data of Ong et al. [26] (dark blue symbols) and Tascini et al. [24] (light blue symbols with $F = 1$) are also included. Our MD data, and those of Ong, and Tascini are compared with Eqs. 8 and 9 (red dashed lines and black dashed lines, respectively).

The normalized interfacial thermal conductance of gold nanoparticles as a function of their radius for the three wetting regimes is illustrated in Fig. 3b. The normalized interfacial thermal conductance corresponds to the conductance divided by its maximal value, $\tilde{G}_k = G_k(R_{np}, \theta)/G_k^{(\max)}(\theta)$ with θ the contact angle in each case. The data of Tascini et al. [24] concerning the size-dependent conductance of gold nanoparticles in a Lennard-Jones fluid, and the data of Ong et al. [26] corresponding to an array crystal, are also included. Fig. 3b confirms that the quadratic expression, Eq. 8, of the acoustic model gives a good description of the data of Tascini et al. and Ong et al. The empirical linear model also provides a good description of such data, as already noticed in [24, 26].

Two observations regarding the value of the length δ are important to remark. Firstly, the absolute value of δ is approximately of the same order of magnitude as that of the water-molecule radius, which is consistent with the fact that the size effects of the thermal conductance are

fitting	$G_k(\infty)$ (MW/K m^2)	δ (nm)
strongly wetting		
quadratic (acoustic)	143.79 ± 3.10	0.10 ± 0.01
linear (empirical)	142.58 ± 3.24	0.21 ± 0.03
intermediate wetting		
quadratic (acoustic)	90.75 ± 1.31	0.05 ± 0.01
linear (empirical)	90.53 ± 1.34	0.11 ± 0.02
weakly wetting		
quadratic (acoustic)	49.95 ± 1.19	0.15 ± 0.01
linear (empirical)	49.18 ± 1.43	0.34 ± 0.04

TABLE I: Parameters of the quadratic (Eq. 8) and linear (Eq. 9) models.

noticeable only for small nanoparticles ($R_{\rm np} < 2$ nm). Secondly, for all the wetting regimes investigated in this work, we find $\delta > 0$, indicating that the thermal conductance increases when the nanoparticle size decreases. This result is consistent with the study of Tascini et al. [24] and Ong et al. [26], but is different from the work of Neidhart et al. [23], who reported the opposite behavior $\delta < 0$, i.e the thermal conductance decreases for small nanoparticles.

2. Relation thermal conductance-fluid density

It is generally argued that the thermal interface conductance G_k is strongly correlated with the density of the fluid at the interface [36, 37]. For a graphene-water system, this relation is described by $G_k(\rho_p) = (\rho_p + B)/A$, where ρ_p is the first peak of the fluid density profile, and A and B are two constants which depend of the system type. We should mention, however, that the correspondence between the interface conductance and the fluid density is not universal, and may even break down as discussed in [37–39].

To discuss the relevance of the relation between the interfacial thermal conductance G_k and the fluid density ρ_p, we have analyzed the behavior of G_k as a function of ρ_p. Fig. 4a shows the first peak of the water density in terms of the nanoparticle radius under a steady heat flow situation. It is observed that for small nanoparticles, the amplitude of the first peak increases. The size dependence of the density of the water layer surrounding the nanoparticle is well described with the functional form $\rho_p(R_{\rm np}) = A\exp(-BR_{\rm np}) + C$. This form describes an exponential decay of the fluid density with the radius of the nanoparticle, leading to $\rho(R_{\rm np}) = C$ when

$R_{\rm np} \to \infty$. This result is qualitatively different from a similar study [40], where the density of the nanolayer for spherical Ag nanoparticles increases as the radius of the nanoparticle increases, reaching a fixed value in the flat-interface limit. The authors of [40] propose a relation between the density of the nanolayer and the diameter of the nanoparticle $D_{\rm np} = 2R_{\rm np}$ taking the form $\rho(D_{\rm np})_p = a\exp(-b/D_{\rm np}^c)$ where a, b and c are constants. In our gold-water system, the exponent of $D_{\rm np}$ is $c = -1$ and we have an independent constant associated with the density of the nanolayer of the corresponding flat surface.

In the following lines we discuss the relation between G_k and ρ_p. Figs. 4b and 4c exhibit the interfacial thermal conductance as a function of the water nanolayer density ρ_p. Our results show that, for a fixed nanoparticle radius $R_{\rm np}$, the evolution of G_k with the contact angle (or wetting) is well described by $G_k(\rho_p) = (\rho_p + B)/A$. Such a relation changes to $G_k(\rho_p) = (\rho_p + B')/A'$ ($A \neq A'$ and $B \neq B'$) when the contact angle is fixed, and the diameter changes. Therefore, we conclude that the relation between the interfacial conductance and the first peak density is not universal, and depends on both the nanoparticle curvature and its wetting properties.

B. Interpretation

In order to interpret the size effects of the thermal conductance as represented in Fig. 3, we analyze the different physical quantities that control the interfacial heat transport between the nanoparticle and water.

1. Interfacial potential energy

First, let us consider the potential energy characterizing the gold-water interface. Heat is transferred between these two media through the interaction between the atoms of the nanoparticle and the atoms of the fluid. Fig. 5a shows the potential energy per atom of the nanoparticle due to the interaction with water as a function of the nanoparticle radius. There is a shell around each gold atom with radius 11 Å and all the water molecules inside this radius are considered in the calculation of the potential energy. The total potential energy calculated in this way is divided by the total number of the gold atoms that interact with water.
From Fig. 5a it is observed that the potential energy is lower for small nanoparticles. In addition, at a fixed value of $R_{\rm np}$, the interfacial potential energy is lower for strongly wetting nanoparticles. This result is consistent with the fact that strongly wetting nanoparticles are

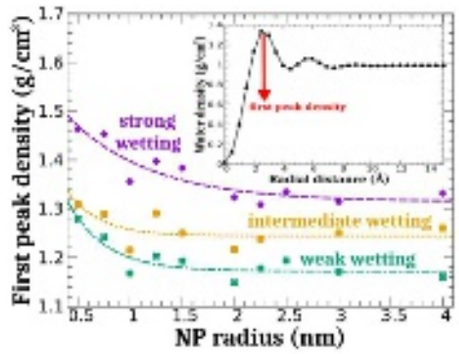

(a)

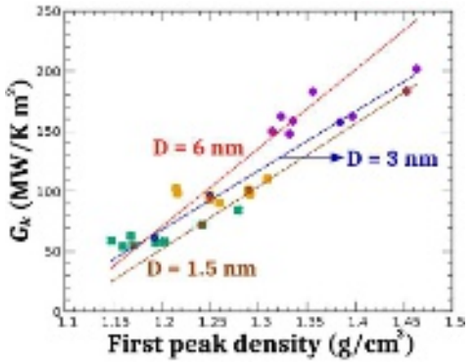

(b)

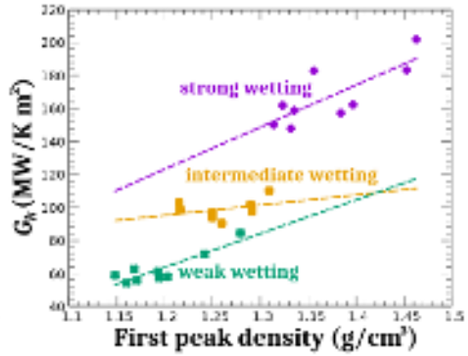

(c)

FIG. 4: Fig. 4a shows the water-solvation first peak as a function of the nanoparticle radius. A typical water density profile around the nanoparticle is shown in the inset. Figs. 4b and 4c show the interfacial thermal conductance as a function of the first density peak for several nanoparticle diameters and for a fixed wetting, respectively. The data are shown for all the nanoparticles sizes in each wetting regime. The function $G_k(\rho_p) = (\rho_p + B)/A$ is also represented in both figures. This function describes the simulation data for the three different wetting regimes and for nanoparticles with diameters $D_{\rm np} = 6, 3$ and 1.5 nm.

characterized by a high work of adhesion, as compared to weakly wetting nanoparticles. Finally, the size dependence of the potential energy is more pronounced for strongly wetting nanoparticles. The more negative potential energy observed for small nanoparticles indicates a stronger bonding of the gold-water interface, which should lead to increased thermal conductance.

The average number of neighbor oxygens, obtained after dividing the total number of gold atoms that interact with water, is shown in Fig. 5b. We observe that the number of neighbors increases for small nanoparticles. Due to these many interactions, the potential energy becomes more negative, partially explaining the behavior outlined in Fig. 5a. After observing Figs. 5a and 5b, we conclude that there is a correlation between the interfacial potential energy and the

number of oxygen neighbors.

Another important observation concerns the relation between the interfacial conductance and the coordination number of the interfacial atoms. The smaller the nanoparticle, the higher the coordination number due to the increased curvature. Also, we observe in Fig. 5c that the thermal conductance increases when the coordination number increases. This conclusion is compatible with the results of Jiang et al. [41], in spite of the fact that they consider different nanoparticle shapes without changing the nanoparticle size, and a different solvent (monoatomic Lennard-Jones fluid). The correlation between the interface conductance and the coordination number seems to have general character regardless of the fluid molecular structure, at least for relatively simple molecular fluids.

2. Density of states

Up to now, we have analyzed the enhancement of the thermal conductance of strongly curved nanoparticles in terms of the potential energy and interface bonding. Interfacial heat transfer depends also on the vibrational density of states (DoS) of the two media. In the following, we examine the DoS of the gold nanoparticle $P_{np}(\omega)$ and of the oxygen atoms of the fluid $P_O(\omega)$. The technical details concerning the DoS calculations are given in the SM.

The most striking feature displayed by the nanoparticle DoS as seen in Fig. 6a is the enhancement of the low frequency peak for small nanoparticles. This peak corresponds to the low frequency van Hove singularity of gold and has been previously observed in other works [23, 42]. As the dimensions of the nanoparticles are reduced, the peak located at the angular frequency ~ 20 ps^{-1} is shifted to lower frequencies. In the SM, a graph can be consulted in which the angular frequency at which the low-frequency peak occurs is plotted, as a function of the diameter of the nanoparticle. These behaviours are also common to the weakly wetting nanoparticle, as seen in the SM. For big nanoparticles, one can observe a second peak at high angular frequency $\sim$ 30 ps^{-1} corresponding to the longitudinal singularity of gold, and this peak is faded out for the 1 nm nanoparticle.

Concerning the DoS characterizing the oxygen atoms, Fig. 6b shows that when the nanoparticle size decreases, firstly the amplitude of the low frequency peak (~ 10 ps^{-1}) is enhanced and secondly, a plateau with structure appears for intermediate frequencies, between 20 s^{-1} and 50 ps^{-1}. This shoulder has been also observed in previous studies [43, 44]. Again, these features

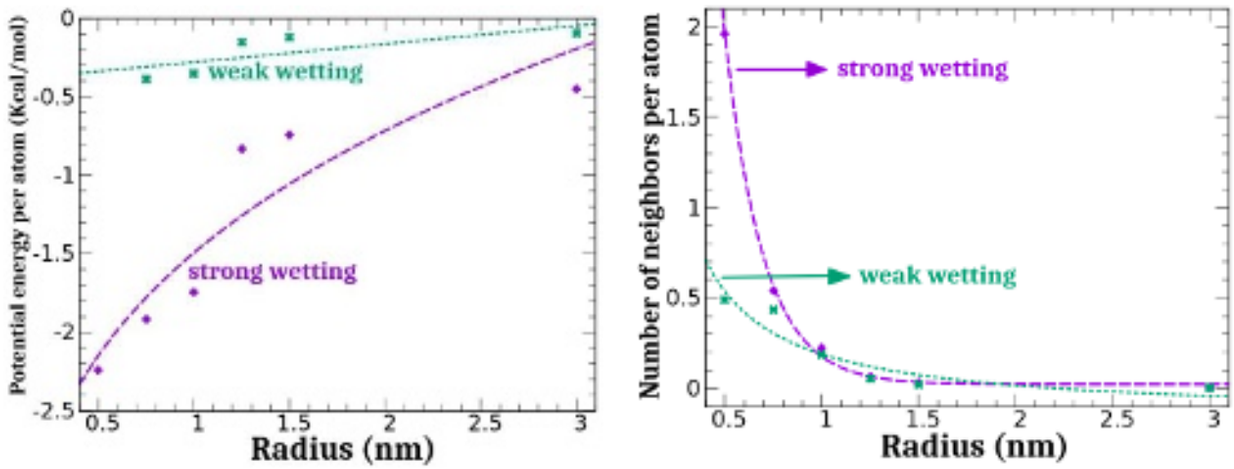

(a) (b)

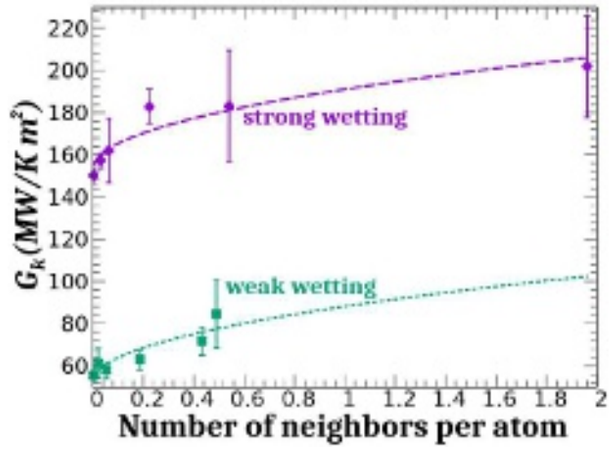

(c)

FIG. 5: Fig. 5a shows, for the different wetting regimes, the potential energy (due to the interaction with water) per gold atom, as a function of the nanoparticle size. Fig. 5b shows the average number of neighbor oxygens of the interfacial gold atoms. Fig. 5c shows the thermal conductance as a function of the number of neighbor oxygens of the interfacial gold atoms.

are also common to the case of weakly wetting nanoparticles, as seen in the SM.

In order to quantify the overlap of vibrational states between two media, we introduce the following quantity [45]:

$$\text{Overlap} = \frac{\int P_{\text{np}}(\omega) P_O(\omega) d\omega}{\int P_{\text{np}}(\omega) d\omega \int P_O(\omega) d\omega} \tag{11}$$

The resulting overlap is presented in Fig. 6c. As the diameter of the nanoparticle decreases, the overlap increases. Such overlap is related to the good matching between the low frequency peak in the nanoparticle DoS (around 12 ps^{-1}) and low frequency peak of oxygen atoms (around

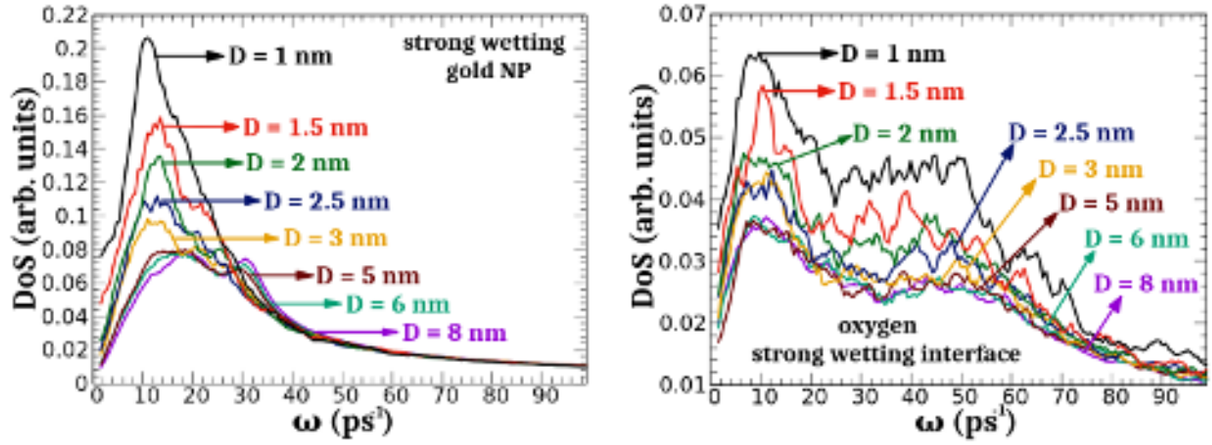

(a) (b)

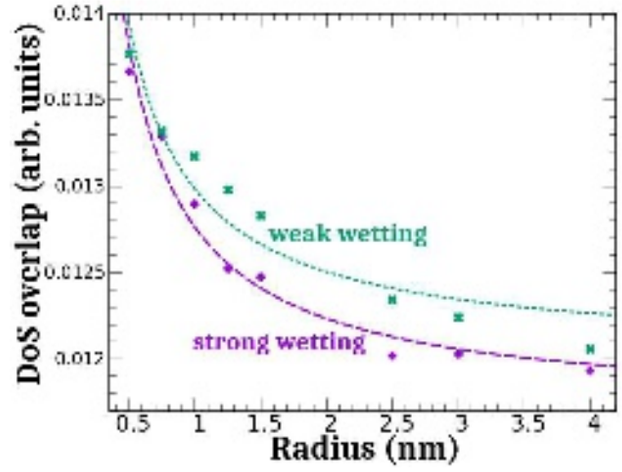

(c)

FIG. 6: Figs. 6a and 6b represent the Density of States (DoS) of the interfacial gold and interfacial oxygen atoms, respectively, for strongly wetting nanoparticles of varying diameters, D. Fig. 6c displays the DoS overlap between the interfacial gold atoms and the oxygen atoms as a function of the nanoparticle radius.

10 ps^{-1}). This enhanced overlap contributes partly to facilitate the interfacial heat transfer between small nanoparticles and liquid water.

3. *Thermal spectrum*

The combined information on the potential energy and the vibrational density of states is encoded in the frequency dependent thermal flux defined as follows [47]:

$$q(\omega) = \frac{2}{A}\mathbf{Re}\left[\sum_{i\in Np}\sum_{j\in Ox}\int_0^{t_{max}}\langle \mathbf{F}_{ij}(\tau)\cdot\mathbf{v}_i(0)\rangle e^{i\omega\tau}d\tau\right], \tag{12}$$

where the real part of the quantity in brackets is considered. The nanoparticle surface area is A, $\mathbf{F}_{ij}$ is the force on the nanoparticle atom i due to the interaction with oxygen j, $\mathbf{v}_i$ the speed of atom i, $\langle \mathbf{F}_{ij}(\tau) \cdot \mathbf{v}_i(0) \rangle$ is the correlation function between $\mathbf{F}_{ij}$ and $\mathbf{v}_i$, τ is the correlation time, and t_{max} is the maximum time. More details concerning the thermal spectrum calculations may be found in the SM.

The frequency-dependent heat flux, $q(\omega)$, gives indication on the frequencies that dominate the interfacial heat transfer. Fig. 7a shows that the thermal spectrum displays a pronounced peak at a frequency 10 ps^{-1}. This peak corresponds to the location of the low frequency peaks displayed by the gold atoms and the oxygen atoms, as discussed before. This correspondance is also illustrated in Fig. 7b where the different DoS have been superimposed to the thermal spectrum. For big nanoparticles, $D > 3$ nm, a second peak in the thermal spectrum may be seen around 30 ps^{-1} which corresponds to the longitudinal peak of gold atoms (see Fig. 6a). These features are found to be qualitatively the same for weakly wetting nanoparticles, as can be seen in the SM. All these considerations highlight the role of low frequency vibrations in the enhanced heat transfer of small nanoparticles.

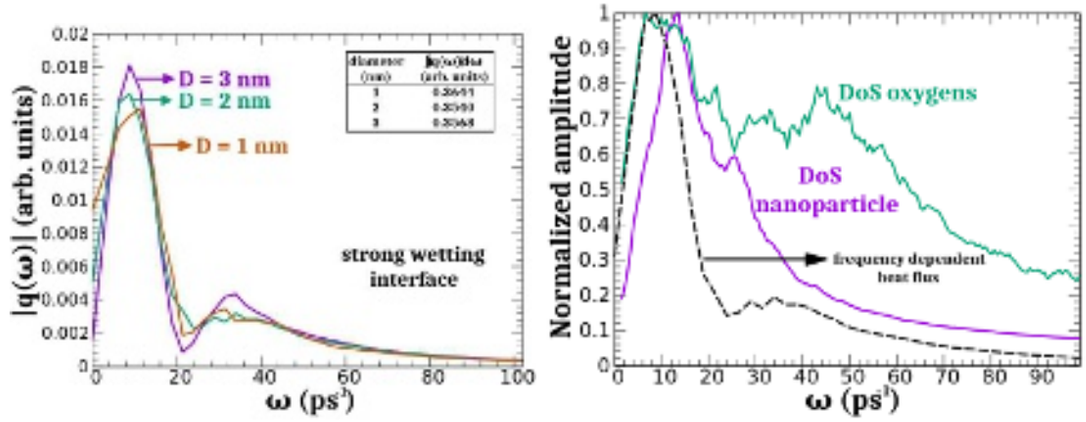

(a) (b)

FIG. 7: Fig. 7a shows the frequency-dependent thermal flux around strongly wetting nanoparticles. The inset show the cumulated heat flux. Fig. 7b compares the thermal spectrum with the DoS of the nanoparticle and the DoS of the oxygen atoms. These latter spectra correspond to a strongly wetting nanoparticle with diameter $D = 2$ nm.

C. Transient simulations: comparison with the continuum model

Once we determined the size dependent thermal conductance, we assess here the accuracy of continuous heat equations model to describe heat transfer around very small nanoparticles heated at high temperatures. To this end, we use transient molecular dynamics of small nanoparticles initially heated up at different temperatures and free to cool down, as described in Section II C. The nanoparticles have diameters ranging from 1 to 3 nm, and have either strong wetting or weak wetting characters.

We consider the following continuum medium model for the nanoparticle and water. The heat diffusion equation and the initial condition for the nanoparticle are:

$$\frac{\partial^2(rT_{\rm np})}{\partial r^2} = \frac{1}{\alpha_{\rm np}}\frac{\partial(rT_{\rm np})}{\partial t}, \qquad \frac{\partial T_{\rm np}(r,t)}{\partial r}|_{r=0} = 0, \qquad T_{\rm np}(r,0) = T_{\rm np0}. \tag{13}$$

The boundary condition between the nanoparticle and the water at the interface is given by the expression:

$$-\lambda_{\rm np}\frac{\partial T_{\rm np}(r,t)}{\partial r}|_{r=R_{\rm np}} = G_k\left(T_{\rm np}(R_{\rm np},t) - T_{\rm w}(R_{\rm np},t)\right).$$

On the other side, the heat diffusion equation and the initial condition for water are:

$$\frac{\partial^2(rT_{\rm w})}{\partial r^2} = \frac{1}{\alpha_{\rm w}}\frac{\partial(rT_{\rm w})}{\partial t}, \qquad T_{\rm w}(r\to\infty,t) = T_{\rm w0}, \qquad T_{\rm w}(R_{\rm np},0) = T_{\rm w0}. \tag{14}$$

The boundary condition between the nanoparticle and the water at the interface satisfies the following expression:

$$\lambda_{np}\frac{\partial T_{\rm np}(r,t)}{\partial r}|_{r=R_{\rm np}} = \lambda_{\rm w}\frac{\partial T_{\rm w}(r,t)}{\partial r}|_{r=R_{\rm np}}$$

$T_{\rm np}(r,t)$ is the temperature of the nanoparticle at a distance r and time t, $\alpha_{\rm np}$ is the nanoparticle thermal diffusivity, $R_{\rm np}$ is the nanoparticle radius, and λ_{np} its thermal conductivity. Similar definitions of T_w and α_w are adopted for water. The thermal diffusivities are defined by $\alpha = \lambda/(\rho c_p)$, where λ is the thermal conductivity, ρ is the density, and c_p the specific heat capacity. The value $T_{\rm np0}$ is the initial temperature of the nanoparticle.

A finite-difference method is employed to solve the coupled Eqs. 13 and 14. The thermophysical parameters of the fluid and the nanoparticle are provided in Table II. We also use the values of G_k determined in a previous section, which were reported in Fig. 3. We focus attention on the temperature evolution of water at a distance of 4 Å from the nanoparticle surface. The predictions of the continuum model together with the molecular dynamics data are depicted in Fig. 8.

Parameter	Value	Reference
$\lambda_{\rm np}$	1.7 W/(m K)	[42, 48, 49]
$\lambda_{\rm w}$	1.01 W/(K m)	[50]
$c_{p,np}$	129 J/(K kg)	[51]
$c_{p,w}$	4184 J/(K kg)	[52]
$\rho_{\rm np}$	19.3 g/cm^3	[53]
ρ_w	–	MD data

TABLE II: Physical parameters of the continuum model.

The cooling time increases with the nanoparticle size, as can be consulted in the SM. The cooling time is longer for weakly wetting nanoparticles than for strongly wetting nanoparticles. For example, for the 3 nm nanoparticles we have 20 - 30 ps difference in the cooling time for initial temperatures of 600 and 1200 K. We also observe one order of magnitude difference in the cooling time of the 1 and 3 nm nanoparticles for both wetting situations.

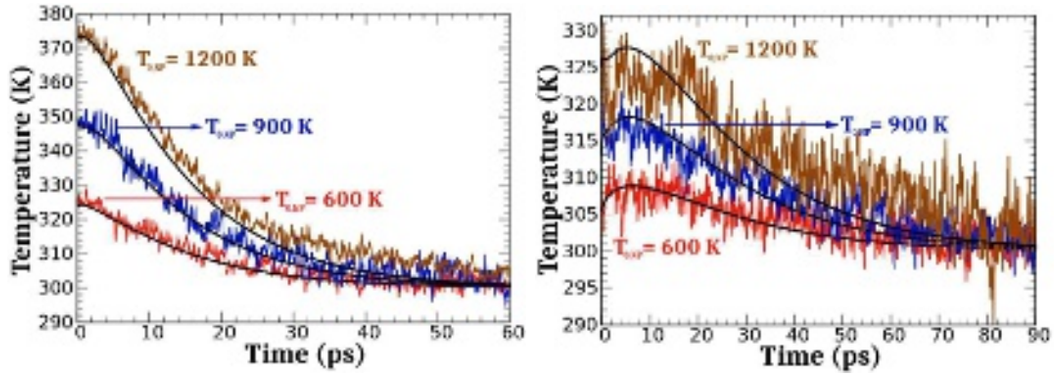

(a) (b)

FIG. 8: Predictions from the continuum model (solid black lines) of the temperature evolution of water at a distance of 4 Å of the nanoparticle surface. Figs. 8a and 8b correspond to the strongly wetting and weakly wetting nanoparticle with diameters of 3 nm, respectively. Three different values of the initial nanoparticle temperatures are considered: 600 K (red data), 900 K (blue data), and 1200 K (brown data).

In order to quantify the deviations between the molecular dynamics data and the predictions

of the continuum model, we introduce the following average:

$$\% \text{ deviation} = \frac{1}{N}\sum_{t} |1 - \frac{T_{\mathrm{MD}}(t)}{T_{\mathrm{CM}}(t)}| \times 100 \tag{15}$$

where N is the number of MD data collected until the water (at a distance 4 Å of the nanoparticle) cools down reaching the temperature < 301 K according to the continuum model, $T_{\mathrm{CM}}(t)$. The temperature $T_{\mathrm{MD}}(t)$ is the temperature obtained from the MD data.

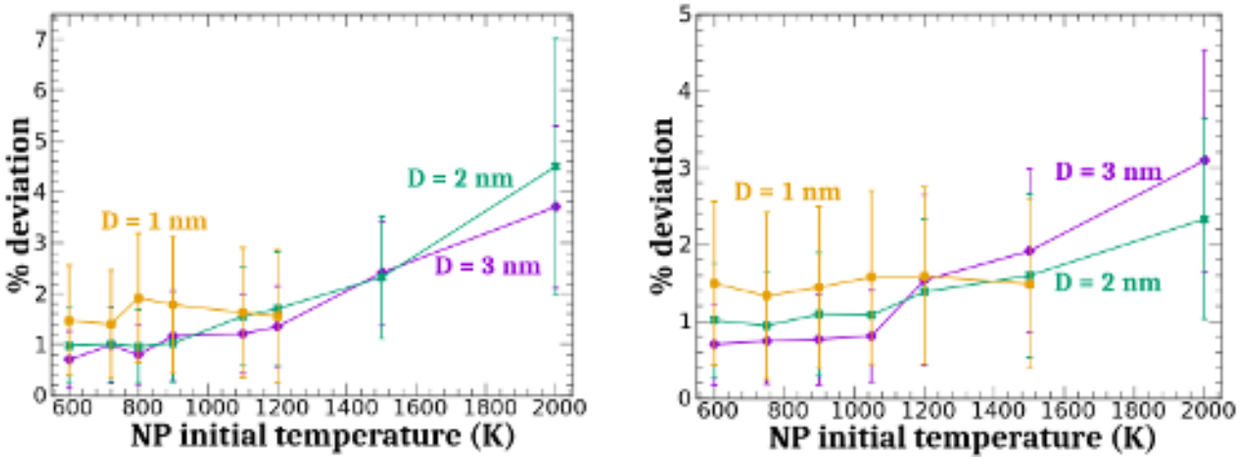

(a) (b)

FIG. 9: Deviations between the continuum model temperature and the molecular dynamics temperature, as given by Eq. 15, during the cooling stage of the water molecules surrounding the nanoparticle in the vicinity of 4 Å from the nanoparticle surface. Different initial temperatures of the nanoparticle, with three different diameters were considered. Fig. 9a corresponds to the strongly wetting case, and Fig. 9b to the weakly wetting case.

Fig. 9 shows the deviations between the T_{MD} and T_{CM}. The deviations increase with the initial nanoparticle temperature, without exceeding 5% in any of the considered cases. For the smallest nanoparticle, the deviations are almost constant and independent of the initial temperature.

When the initial temperature of the 2 and 3 nm nanoparticles is above 2000 K, the nanoparticles melt down within an interval of 40 ps. The melting point of a 3 nm gold nanoparticle is known to be between 800 - 900 K [17, 54, 55], while that of the bulk is approximately 1300 K. For the 1 nm nanoparticle, an initial temperature higher than 1500 K melts the strongly wetting nanoparticle and higher than 1200 K melts the weakly wetting case. An exhaustive study of nanoparticle melting and fragmentation is beyond the scope of the present article.

Nevertheless, we conclude that continuum models can describe heat transfer around very small nanoclusters (down to $R_{\rm np} = 1$ nm) heated up at temperatures below the fragmentation point.

IV. CONCLUSION

In conclusion, we have investigated the dependence of the interface thermal conductance of gold nanoparticles with the nanoparticle size. The thermal conductance increases by decreasing the nanoparticle radius, whatever the wetting properties of the interface are. The size-effects of the thermal transport were rationalized from the perspective of an acoustic model. It was concluded that the thermal conductance increases when the nanoparticle size decreases, following the relation $G_k(R_{\rm np}) = G_K(\infty)(1 + \delta/R_{\rm np})^2$. Such an expression describes not only the thermal conductance of gold nanoparticles-water interfaces, but other curved interfaces as well [24, 26]. The size dependence of the thermal conductance may be described by the empirical relation proposed in [24], $G_k(R_{np}) = G_k(\infty)(1 + \delta/R_{np})$.

The increase of the conductance with the nanoparticle curvature may be due to two important factors. First, when the nanoparticle size is reduced, the number of water molecules interacting with a surface gold atom increases, as quantified by the water-gold potential energy. Second, when the nanoparticle size is reduced, the spectrum of the vibrational density of states is strongly modified. In particular, the spectrum of large nanoparticles displays two van Hove peaks corresponding to the density of states of the bulk medium. The high frequency peak vanishes by reducing the nanoparticle radius, while the low frequency peak is enhanced. This enhancement explains the energy transfer between small gold nanoparticles and the liquid water, where the spectrum of the oxygen matches the nanoparticle low frequency peak.

Finally, we have assessed the extent to which continuum heat equations correctly describe the cooling kinetics of small nanoparticles initially heated up at high temperatures. Continuum medium models are found to describe well the heat transfer of a broad range of nanoparticle sizes with diameters down to 1 nm, and heated up to hundredths of Kelvins.

Our acoustic model to understand size-dependent effects on the thermal conductance, may be extended to describe systems well beyond plasmonic nanoparticles in water. The size effects evidenced here should be important for nanocomposites and also nanocrystals. Also,

beyond the linear regime studied here, the fragmentation process of small nanoparticles, and in particular the influence of wetting, may be systematically explored [56].

V. SUPPLEMENTARY MATERIAL

The supplementary material describes : 1) the data collection and analysis of the molecular dynamics data 2) the details of the density of states and thermal spectrum calculations 3) the density of states and thermal spectrum characterizing weakly wetting nanoparticles 4) the analysis of nanoparticle cooling times based on the continuous heat transfer model.

VI. ACKNOWLEDGMENTS

OGV acknowledges CONACyT-México (CVU Num. 862921) for financial support in obtaining the Ph. D. degree, and the IDEXLYON program for supporting a visit to the Université de Lyon. OGV, SM, and RS acknowledge support from the PSMN (Pôle Scientifique de Modélisation Numérique) of the ENS de Lyon, France for the computing resources.

[1] J. Veilleux and S. Coulombe; A dispersion model of enhanced mass diffusion in nanofluids; Chemical Engineering Science **66** (11); pp. 2377–2384; 2011.

[2] S. Komati and A. K. Suresh; Anomalous Enhancement of Interphase Transport Rates by Nanoparticles: Effect of Magnetic Iron Oxide on Gas-Liquid Mass Transfer; Industrial & Engineering Chemistry Research **49** (1); pp. 390–405; 2010.

[3] W. Zhao and J. M. Karp; Nanoantennas heat up; Nature Materials **8** (6); pp. 453–454; 2009.

[4] N. Ali, J. A. Teixeira, and A. Addali; A Review on Nanofluids: Fabrication, Stability, and Thermophysical Properties; Journal of Nanomaterials; pp. 1–33; 2018.

[5] D. P. Kulkarni, D. K. Das, and R. S. Vajjha; Application of nanofluids in heating buildings and reducing pollution; Applied Energy **86** (12); pp. 2566–2573; 2009.

[6] S. Wippermann, M. Vörös, D. Rocca, A. Gali, G. Zimanyi, and G. Galli; High-Pressure Core Structures of Si Nanoparticles for Solar Energy Conversion; Physical Review Letters **110** (4); 046804; 2013.

[7] R. Taylor, S. Coulombe, T. Otanicar, P. Phelan, A. Gunawan et al.; Small particles, big impacts: A review of the diverse applications of nanofluids; Applied Physics Reviews **113** (1); 011301; 2013.

[8] J. N. Solanki and Z. V. P. Murthy; Preparation of Silver Nanofluids with High Electrical Conductivity; Journal of Dispersion Science and Technology **32**; pp. 724–730; 2011.

[9] A. Plech and V. Kotaidis; Laser-induced heating and melting of gold nanoparticles studied by time-resolved x-ray scattering; Physical Review B **70** (19); 195423; 2004.

[10] V. Kotaidis, C. Dahmen, G. von Plessen, F. Springer, and A. Plech; Excitation of nanoscale vapor bubbles at the surface of gold nanoparticles in water; The Journal of Chemical Physics **124** (18); 184702; 2006.

[11] Z. Ge, D. G. Cahill, and P. V. Braun; AuPd Metal Nanoparticles as Probes of Nanoscale Thermal Transport in Aqueous Solution; The Journal of Physical Chemistry B **108** (49); pp. 18870–18875 (2004).

[12] X. Wu, Y. Ni, J. Zhu, N. D. Burrows, C. J. Murphy, T. Dumitrica and X. Wang; Thermal transport across surfactant layers on gold nanorods in aqueous solution; ACS Appl. Mater. Interfaces **8**; pp. 10581–10589; 2016.

[13] A. J. Schmidt, J. D. Alper, M. Chiesa, G. Chen, S. K. Das, and K. Hamad-Schifferli; Absorption and thermal decay; J. Phys. Chem. C **112**; pp. 13320–13323; 2008.

[14] J. Park and D. G. Cahill, Plasmonic sensing of heat transport at solid-liquid interfaces, J. Phys. Chem. C **120** 2814-2821 (2016).

[15] T. Stoll, P. Maioli, A. Crut, S. Rodal-Cedeira, I. Pastoriza-Santos, F. Vallée and N. Del Fatti; Time-resolved investigations of the cooling dynamics of metal nanoparticles: impact of environment; J. Phys. Chem. C **119**; pp. 12757–12764; 2015.

[16] S. Merabia, S. Shenogin; L. Joly, P. Keblinski, and J.-L. Barrat; Heat transfer from nanoparticles: A corresponding state analysis; Proceedings of the National Academy of Sciences **106** (36); pp. 15113–15118; 2009.

[17] X. Chen, A. Munjiza, K. Zhang, and D. Wen; Molecular Dynamics Simulation of Heat Transfer from a Gold Nanoparticle to a Water Pool; The Journal of Physical Chemistry C 118 (2); pp. 1285–1293; 2014.

[18] V. Juve, A. Crut, P. Maioli, M. Pellarin, M. Broyer, N. DelFatti and F. Vallée; Probing elasticity at the nanoscale: Terahertz acoustic vibration of small metal nanoparticles; NanoLetters **10**; pp. 1853–1858; 2010.

[19] A. Rajabpour, R. Seif, S. Arabha, M. M. Heyhat, S. Merabia, and A. Hassanali; Thermal transport at a nanoparticle-water interface: A molecular dynamics and continuum modeling study; The Journal of Chemical Physics **150** (11); 114701; 2019.

[20] J.-H. Pu, J. Sun, W. Wang and H. S. Wang; Generation and evolution of nanobubbles on heat nanoparticles: a molecular dynamics study; Langmuir **36**; pp. 2375–2382; 2020.

[21] C. Z. Zhao, W. An, Y. Zhang, Q. Dong and N. Gao; A molecular dynamics analysis on interfacial thermal resistance between particle and medium in light-induced heat transfer of plasmonic nanofluid; Langmuir **38**; pp. 2327–2334; 2022.

[22] A. R. Nair and S. P. Sathian; Heat transfer across nanoparticle liquid interfaces, Journal of Heat Transfer **139**; 112402; 2016.

[23] S. M. Neidhart and J. D. Gezelter; Thermal Transport is Influenced by Nanoparticle Morphology: A Molecular Dynamics Study; The Journal of Physical Chemistry C **122**; pp. 1430–1436; 2018.

[24] A. S. Tascini, J. Armstrong, E. Chiavazzo, M. Fasano, P. Asinari, and F. Bresme; Thermal transport across nanoparticle-fluid interfaces: the interplay of interfacial curvature and nanoparticle-fluid interactions; Physical Chemistry Chemical Physics **19** (4); pp. 3244–3253; 2017.

[25] M. Roodbari, M. Abbasi, S. Arabha, A. Gharedaghi, and A. Rajabpour; Interfacial thermal conductance between TiO2 nanoparticle and water: a molecular dynamics study; Journal of Molecular Liquids **348**; 118053; 2022.

[26] W.-L. Ong, S. Majumdar, J. A. Malen and A. J. H Mc Gaughey; Coupling of organic and inorganic vibrational states and their thermal transport in nanocrystals arrays; Journal of Physical Chemistry C **118**; pp. 7288–7295; 2014.

[27] A. Lervik, F. Bresme and S. Kjelstrup; Heat transfer in soft nanoscale interfaces: the influence of interface curvature; Soft Matter **5**; pp. 2407–2414; 2009.

[28] O. Wilhelmsen, T. T. Trinh, S. Kjestrup, S. T. van Erp and D. Bedeaux; Heat and Mass transfer across interfaces in complex nanogeometries; Physical Review Letters **114**; 065901; 2015.

[29] A. M. Karim, N. Al Hasan, S. Ivanov, S. Siefert, R. T. Kelly, et al.; Synthesis of 1 nm Pd Nanoparticles in a Microfluidic Reactor: Insights from in Situ X-ray Absorption Fine Structure Spectroscopy and Small-Angle X-ray Scattering; The Journal of Physical Chemistry C **119** (23); pp. 13257–1326; 2015.

[30] H. Ding and Z. Chen; Nanotheranostic Application of Fluorescent Protein-Gold Nanocluster Hybrid Materials: A Mini-review; Nanotheranostics **5** (4); pp. 461–471; 2021.

[31] S. Merabia, J. Lombard, and A. Alkurdi; Importance of viscoelastic and interface bonding effects in the thermal boundary conductance of solid-water interfaces; International Journal of Heat and Mass Transfer **100**; pp. 287–294; 2016.

[32] R. Prasher; Acoustic mismatch model for thermal contact resistance of van der Waals contacts; Applied Physics Letters **94**; 041905; 2009.

[33] A. Jimenez, A. Sarsa, M. Blazquez and T. Pineda; A molecular dynamics study of the surfactant surface density of alkanethiol self-assembled monolayers on gold nanoparticles as a function of the radius; Journal of Physical Chemistry C **114**; pp. 21309–21314; 2010.

[34] J. L. F. Abascal and C. Vega; A general purpose model for the condensed phases of water: TIP4P/2005; The Journal of Chemical Physics **123** (23); 234505; 2005.

[35] H. Heinz, R. A. Vaia, B. L. Farmer, and R. R. Naik; Accurate Simulation of Surfaces and Interfaces of Face-Centered Cubic Metals Using 12-6 and 9-6 Lennard-Jones Potentials; The Journal of Physical Chemistry C **112** (44); pp. 17281–17290; 2008.

[36] D. Alexeev, J. Chen, J. H. Walther, P. Konstantinos, P. Angelikopoulos, and P. Koumoutsakos; Kapitza Resistance between Few-Layer Graphene and Water: Liquid Layering Effects; Nano Letters **15** (9); pp. 5744–5749; 2015.

[37] L. J. Challis, K. Dransfeld, and J. Wilks; Heat Transfer Between Solids and Liquid Helium II; Proceedings of the Royal Society A: Mathematical, Physical and Engineering Sciences **260** (1300); pp. 31–46; 1961.

[38] H. Han, S. Merabia, F. Müller-Plathe; Thermal Transport at Solid-Liquid Interfaces: High Pressure Facilitates Heat Flow Through Non-Local Liquid Structuring; The Journal of Physical Chemistry Letters **8**; pp. 1946–1951; 2017.

[39] X. Peng, P. Jiang, Y. Ouyang, S. Lu, W. Ren, and J. Chen; Reducing Kapitza Resistance between Graphene/Water Interface via Interfacial Superlattice Structure; Nanotechnology **33**; 035707; 2021.

[40] M.M. Heyhat, A. Rajabpour, M. Abbasi, and S. Arabha; Importance of nanolayer formation in nanofluid properties: Equilibrium molecular dynamic simulations for Ag-water nanofluid; Journal of Molecular Liquids **264**; pp. 699–705; 2020.

[41] M. Jiang, J. D. Olarte-Plata, and F. Bresme; Heterogeneous thermal conductance of nanoparticle-fluid interfaces: an atomistic nodal approach; The Journal of Chemical Physics **156**; 044701; 2022.

[42] X. Chen, A. Munjiza, K. Zhang, and D. Wen; Molecular Dynamics Simulation of Heat Transfer from a Gold Nanoparticle to a Water Pool; The Journal of Physical Chemistry **C 118** (2); pp. 1285–1293; 2014.

[43] U. Balucani, J. P. Brodhot, and R. Vallauri; Analysis of the velocity autocorrelation function of water; Journal of Physics: Condensed Matter **8** (34); pp. 6139–6144; 1996.

[44] C. Rocchi, A. R. Bizzarri, and S. Cannistraro; Water dynamical anomalies evidenced by molecular-dynamics simulations at the solvent-protein interface; Physical Review E **57** (3); pp. 3315–3325; 1998.

[45] J. Lan and B. Li; Thermal rectifying effect in two-dimensional anharmonic lattices; Physical Review B **74** (21); 214305; 2006.

[46] J. Chen, G. Zhang, and B. Li; Tunable thermal conductivity of $Si_{1-x}Ge_x$ nanowires; Applied Physics Letters **95** (7); 073117; 2009.

[47] K. Sääskilahti, J. Oksanen, J. Tulkki, and S. Volz; Spectral mapping of heat transfer mechanisms at liquid-solid interfaces; Physical Review E **93** (5); 052141; 2016.

[48] C. F. Richardson and P. Clancy; Contribution of thermal conductivity to the crystal-regrowth velocity of embedded-atom-method-modeled metals and metal alloys; Physical Review B **45** (21); pp. 12260–12268; 1992.

[49] S. Kuang and J. D. Gezelter; A gentler approach to RNEMD: Nonisotropic velocity scaling for computing thermal conductivity and shear viscosity; The Journal of Chemical Physics **133** (16); 164101; 2010.

[50] F. Römer, A. Lervik, and F. Bresme; Nonequilibrium molecular dynamics simulations of the thermal conductivity of water: A systematic investigation of the SPC/E and TIP4P/2005 model; The Journal of Chemical Physics **137** (7); 074503; 2012.

[51] D. Werner, S. Hashimoto, and T. Uwada; Remarkable Photothermal Effect of Interband Excitation on Nanosecond Laser-Induced Reshaping and Size Reduction of Pseudospherical Gold Nanoparticles in Aqueous Solution; Langmuir **26** (12); pp. 9956–9963; 2010.

[52] Open University (2008). S104 Book 3 Energy and Light, p. 59. The Open University.

[53] Charles E. Ophartd. (2003). Density of Gold. May 2021, from Elmhurst College Web site: http://chemistry.elmhurst.edu/vchembook/125Adensitygold.html

[54] P. Buffat and J.-P. Borel; Size effect on the melting temperature of gold particles; Physical Review A **13** (6); pp. 2287–2298; 1976.

[55] L. J. Lewis, P. Jensen, and J.-L. Barrat; Melting, freezing, and coalescence of gold nanoclusters; Physical Review B **56** (4); pp. 2248–2257; 1997.

[56] H. Huang and L. V. Zhigilei; Atomistic view of laser fragmentation of gold nanoparticles in a liquid environment; J. Phys. Chem. C **125** (24); pp. 13413–13432; 2021.

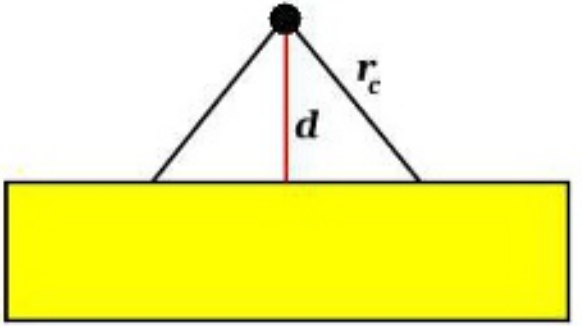

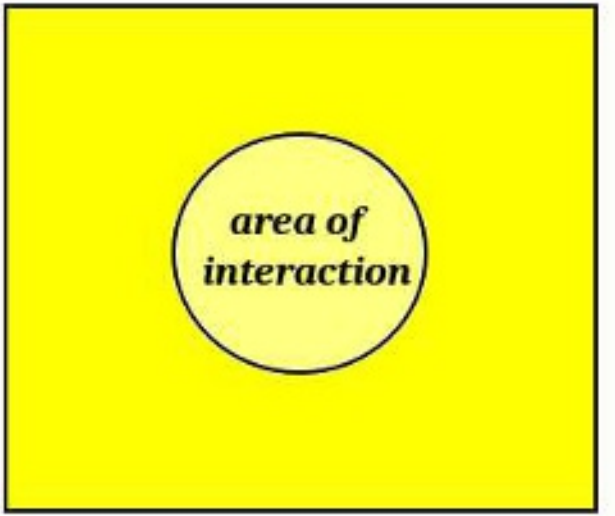

Area of interaction for a planar surface

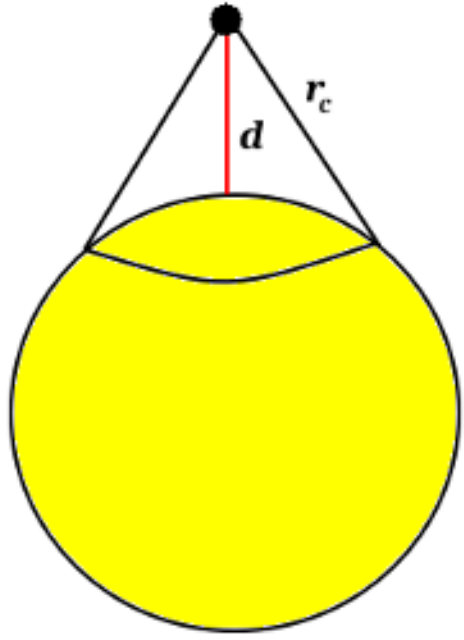

Area of interaction for a spherical surface

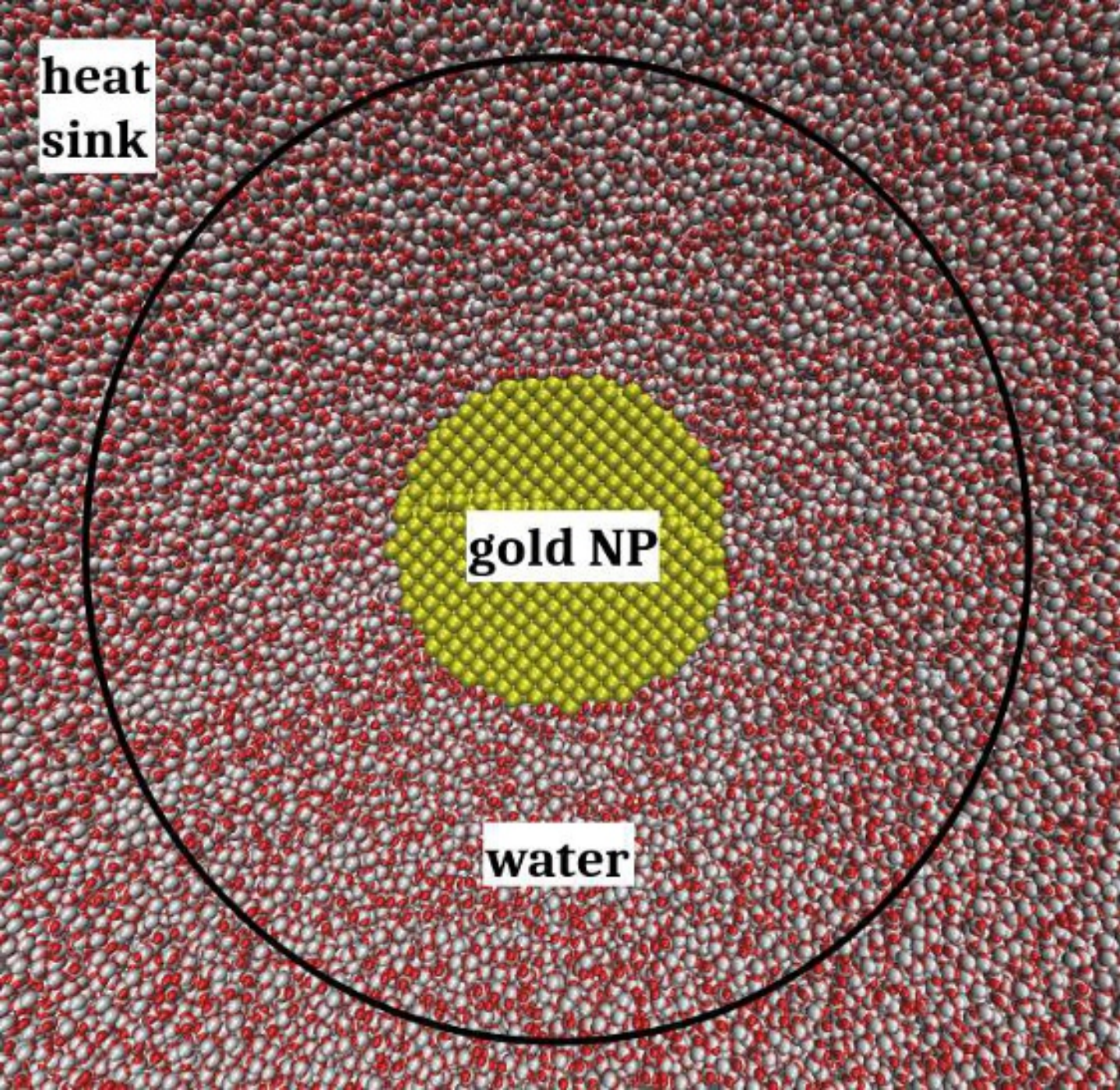
heat
sink
gold NP
water

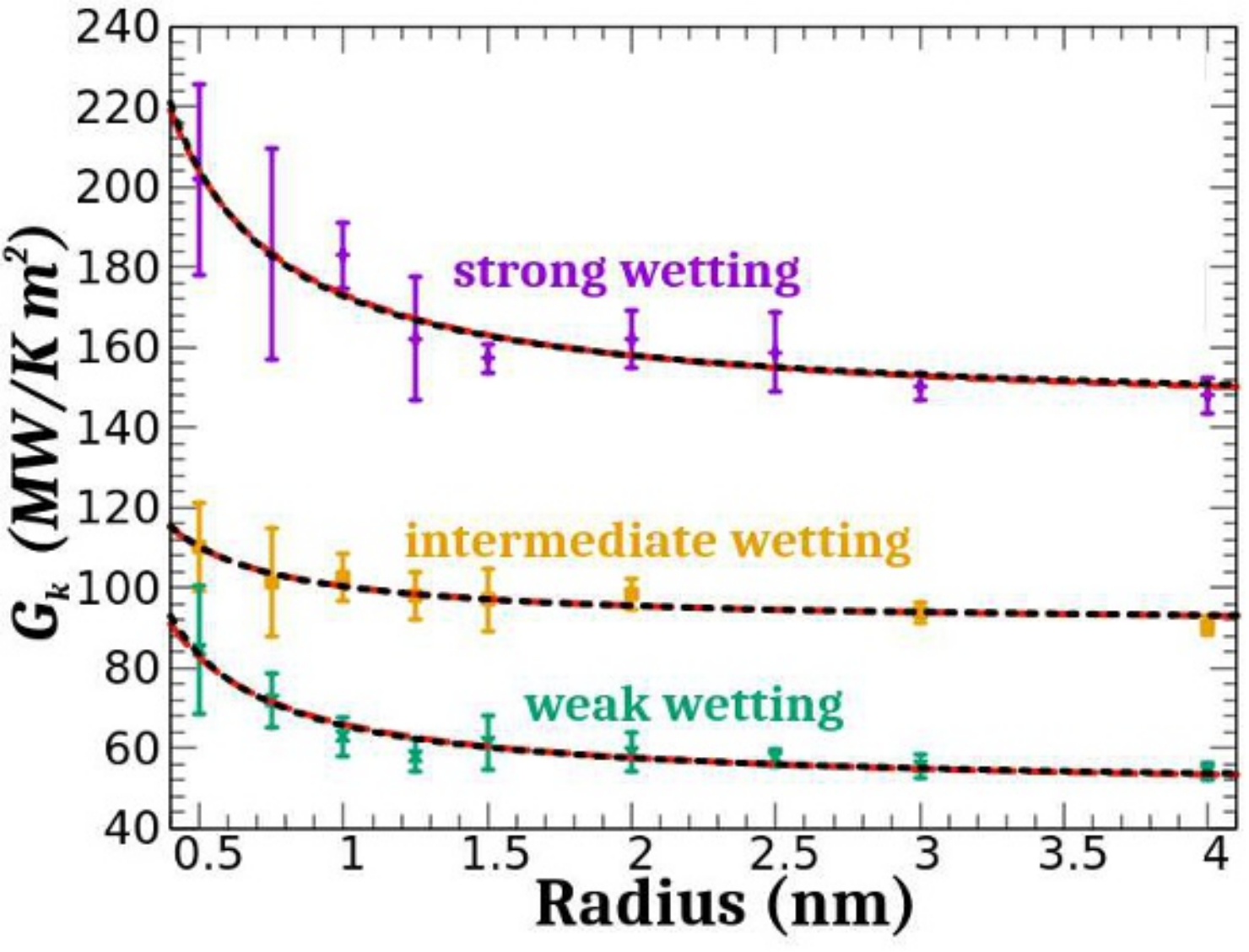
240
220
200
180
160
140
120
100
80
60
40
G_k (MW/K m^2)
strong wetting
intermediate wetting
weak wetting
0.5
1
1.5
2
2.5
3
3.5
4
Radius (nm)

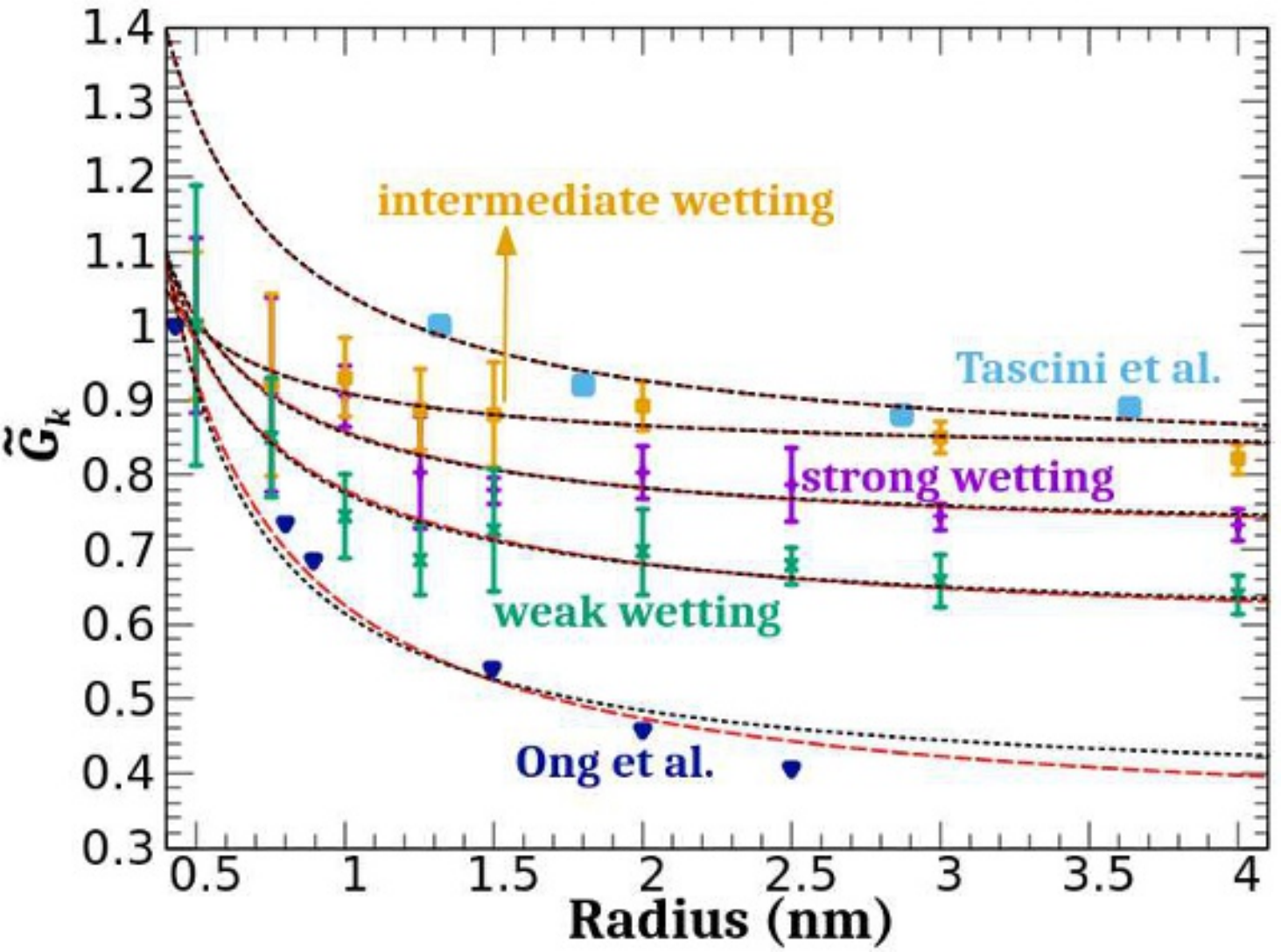
intermediate wetting
Tascini et al.
strong wetting
weak wetting
Ong et al.
$\tilde{G}_k$
Radius (nm)
1.4
1.3
1.2
1.1
1
0.9
0.8
0.7
0.6
0.5
0.4
0.3
0.5
1
1.5
2
2.5
3
3.5
4

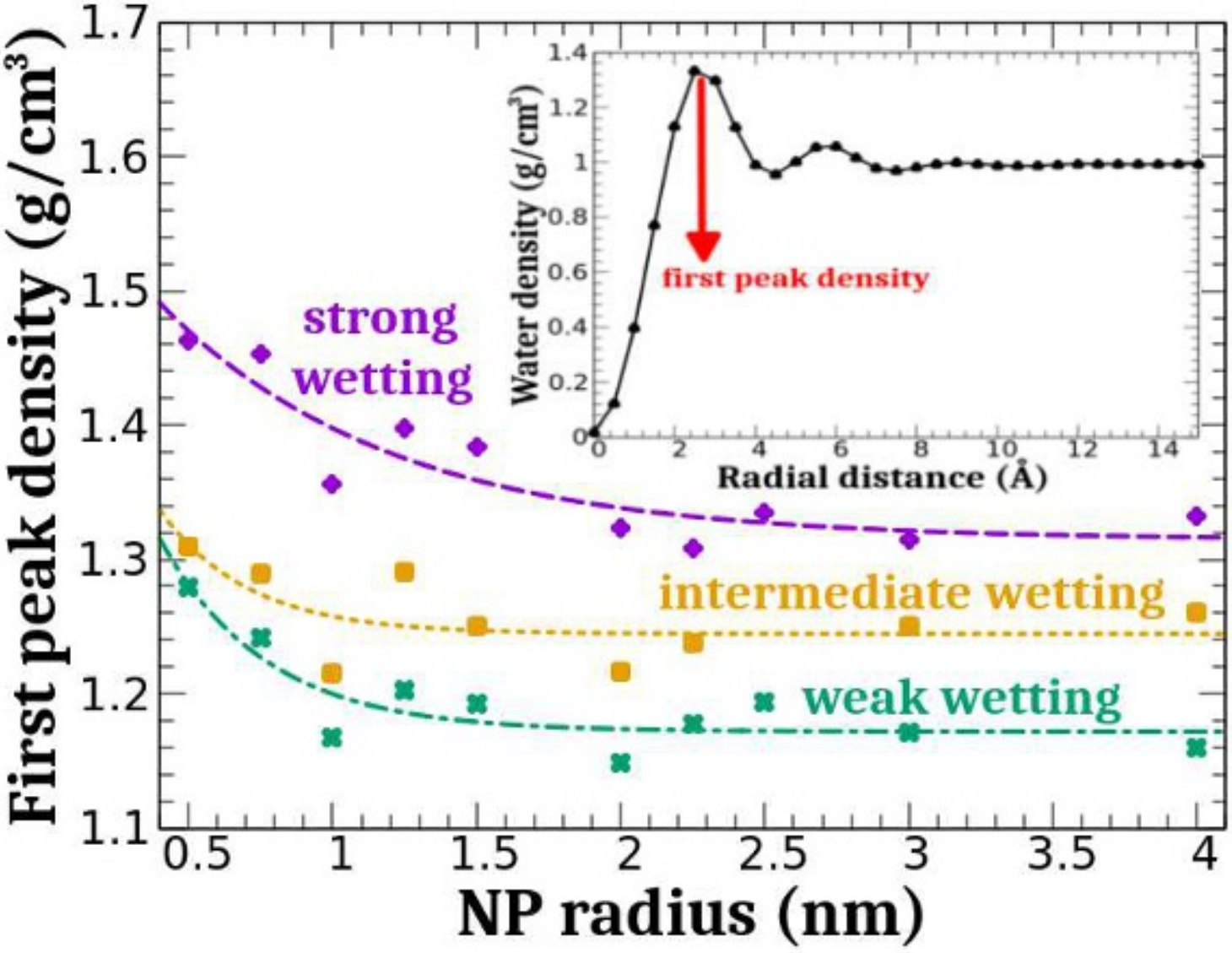
First peak density (g/cm³)
NP radius (nm)
strong wetting
intermediate wetting
weak wetting
Water density (g/cm³)
Radial distance (Å)
first peak density

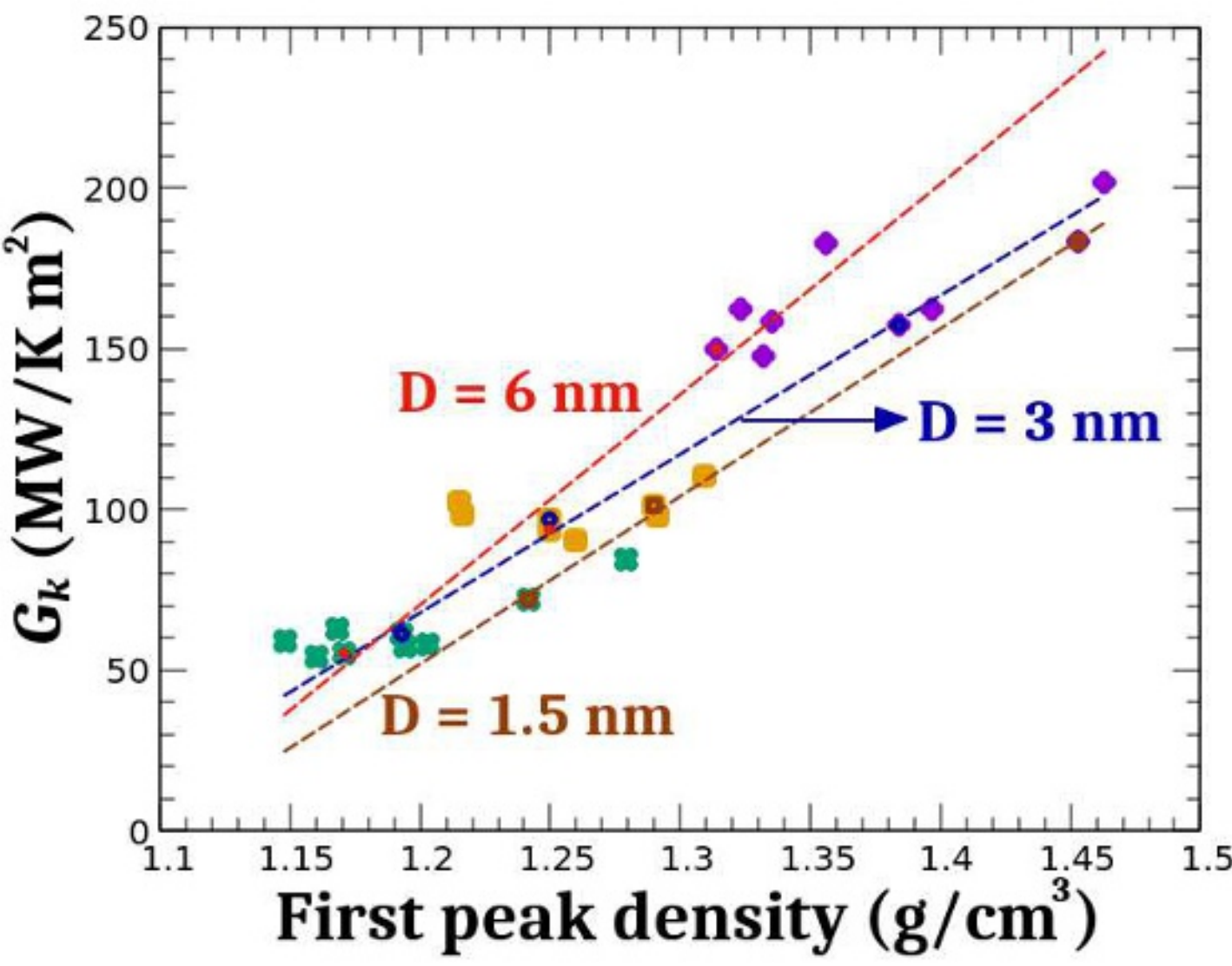
250
200
150
100
50
0
1.1
1.15
1.2
1.25
1.3
1.35
1.4
1.45
1.5
G_k (MW/K m^2)
First peak density (g/cm^3)
D = 6 nm
D = 3 nm
D = 1.5 nm

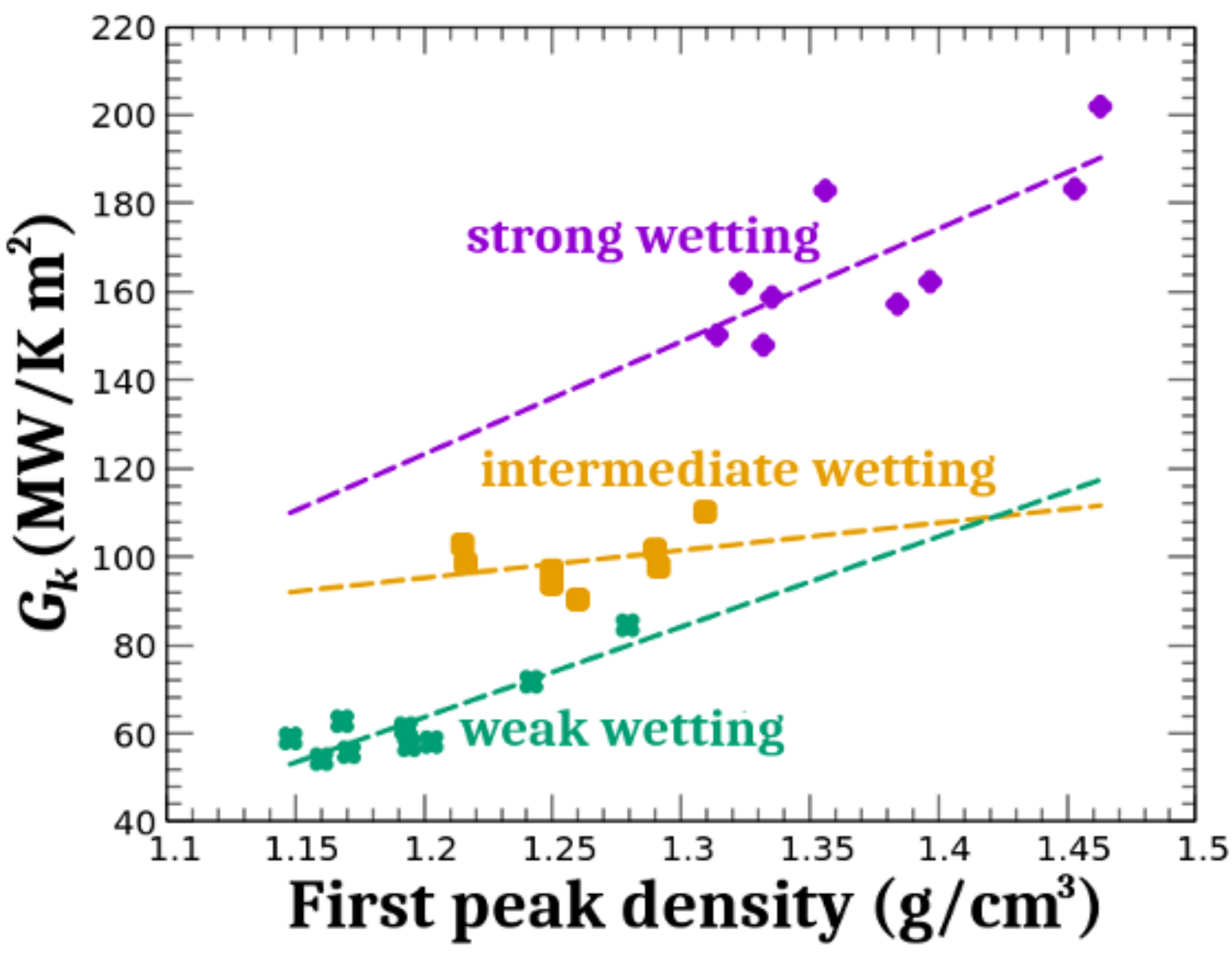
220
200
180
160
140
120
100
80
60
40
G_k (MW/K m^2)
strong wetting
intermediate wetting
weak wetting
1.1
1.15
1.2
1.25
1.3
1.35
1.4
1.45
1.5
First peak density (g/cm^3)

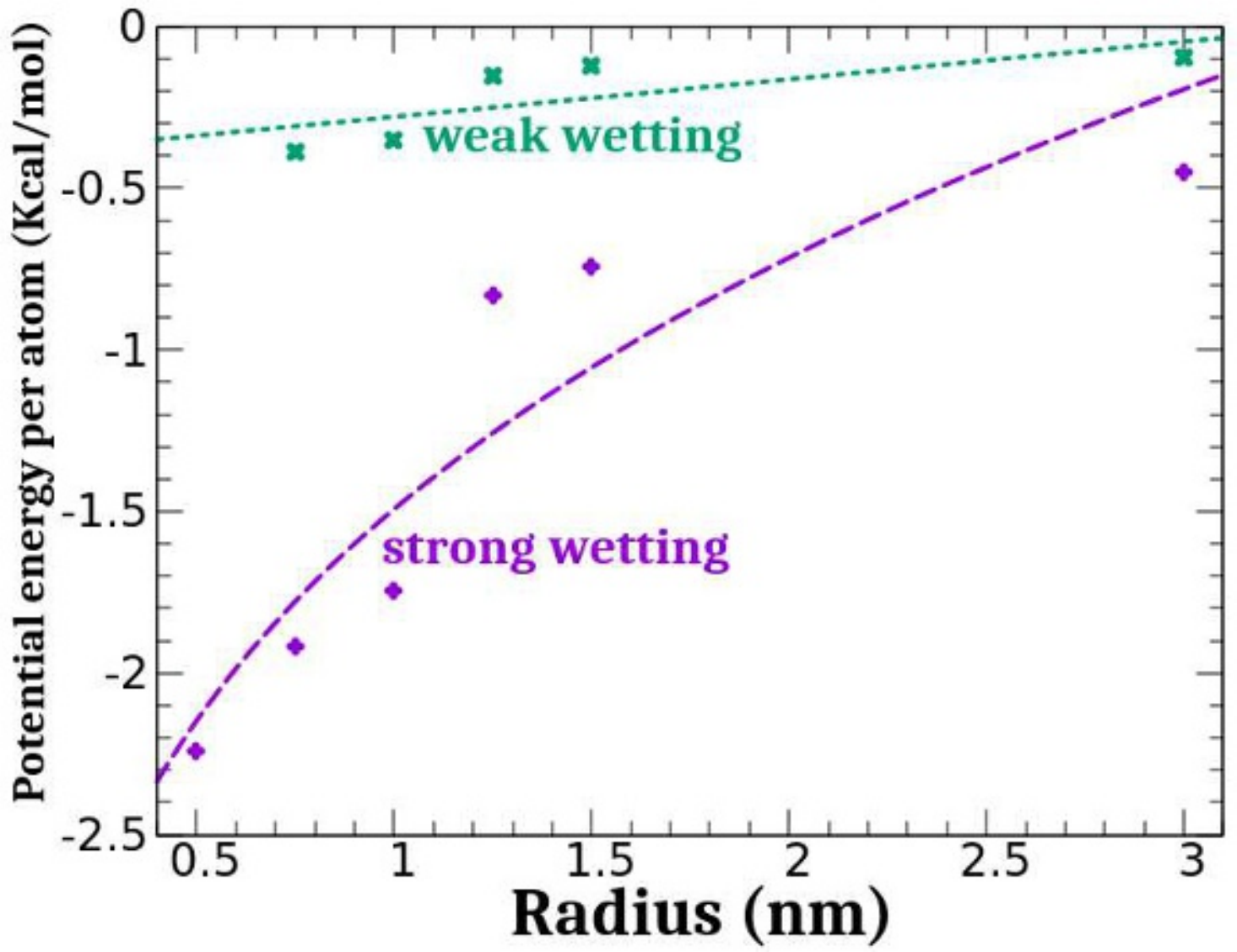
Potential energy per atom (Kcal/mol)
0
-0.5
-1
-1.5
-2
-2.5
0.5
1
1.5
2
2.5
3
Radius (nm)
weak wetting
strong wetting

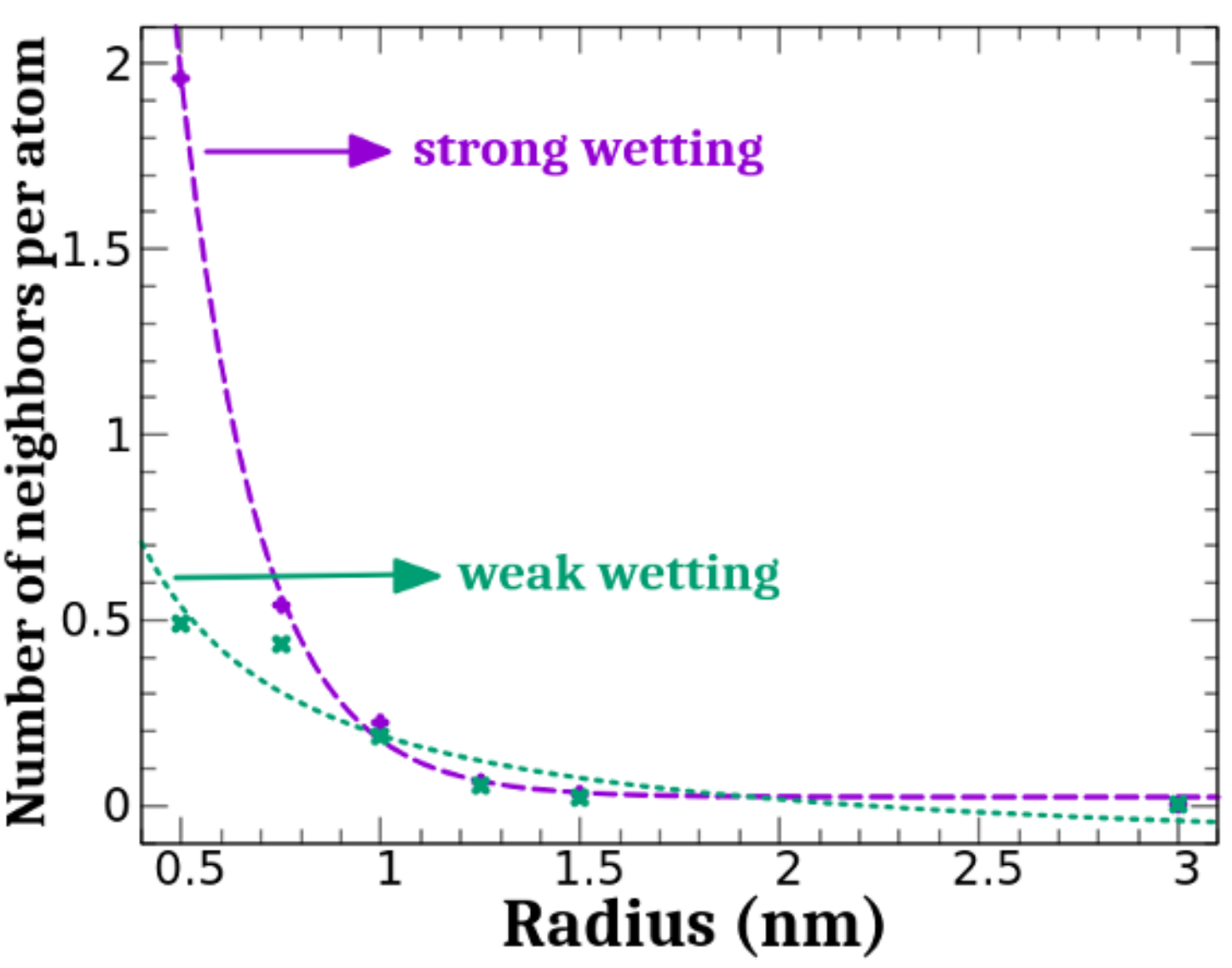
Number of neighbors per atom
Radius (nm)
strong wetting
weak wetting
0
0.5
1
1.5
2
0.5
1
1.5
2
2.5
3

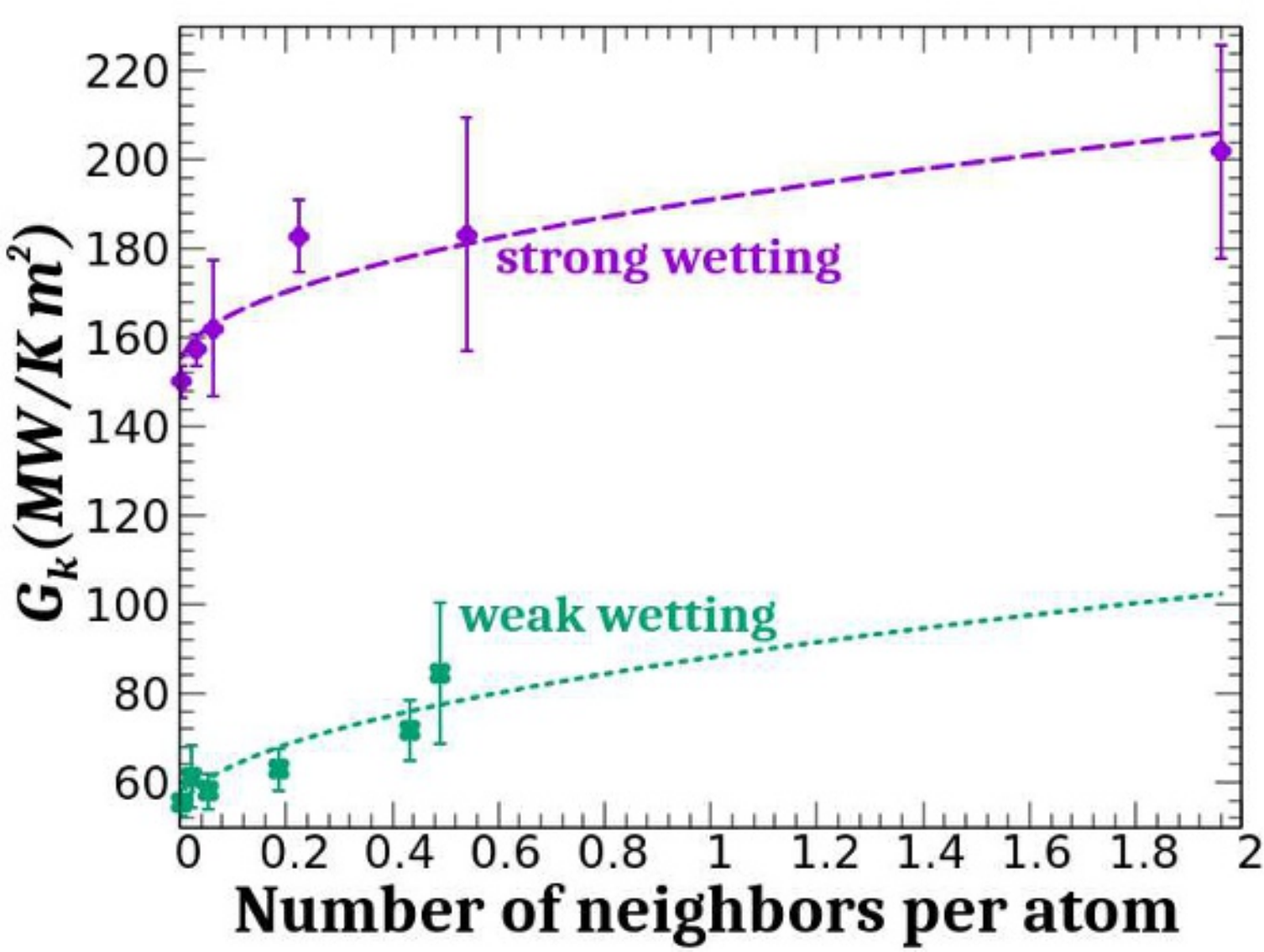
220
200
180
160
140
120
100
80
60
$G_k (MW/K\,m^2)$
strong wetting
weak wetting
0
0.2
0.4
0.6
0.8
1
1.2
1.4
1.6
1.8
2
Number of neighbors per atom

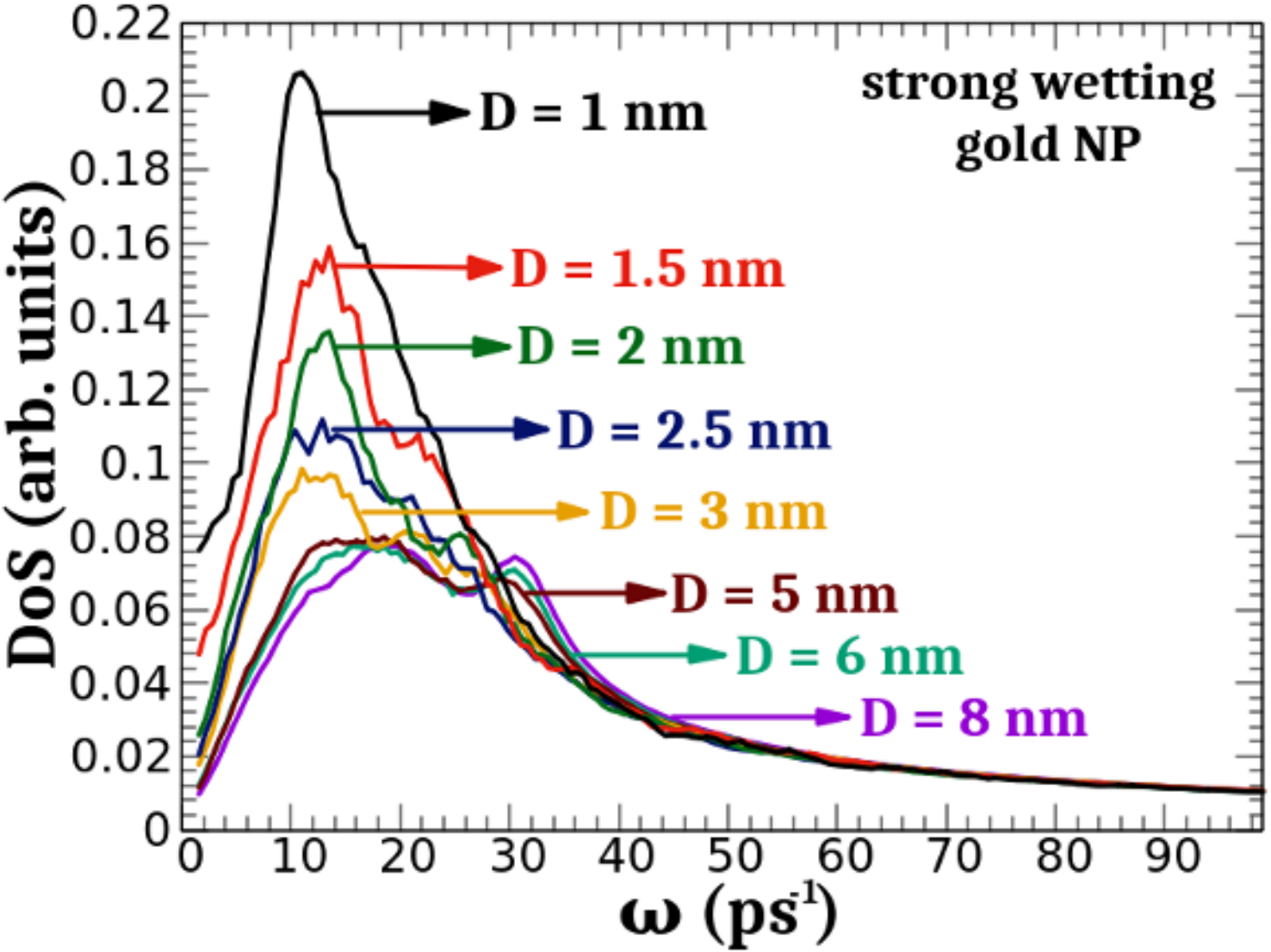
strong wetting
gold NP
D = 1 nm
D = 1.5 nm
D = 2 nm
D = 2.5 nm
D = 3 nm
D = 5 nm
D = 6 nm
D = 8 nm
DoS (arb. units)
ω (ps-1)
0
0.02
0.04
0.06
0.08
0.1
0.12
0.14
0.16
0.18
0.2
0.22
0
10
20
30
40
50
60
70
80
90

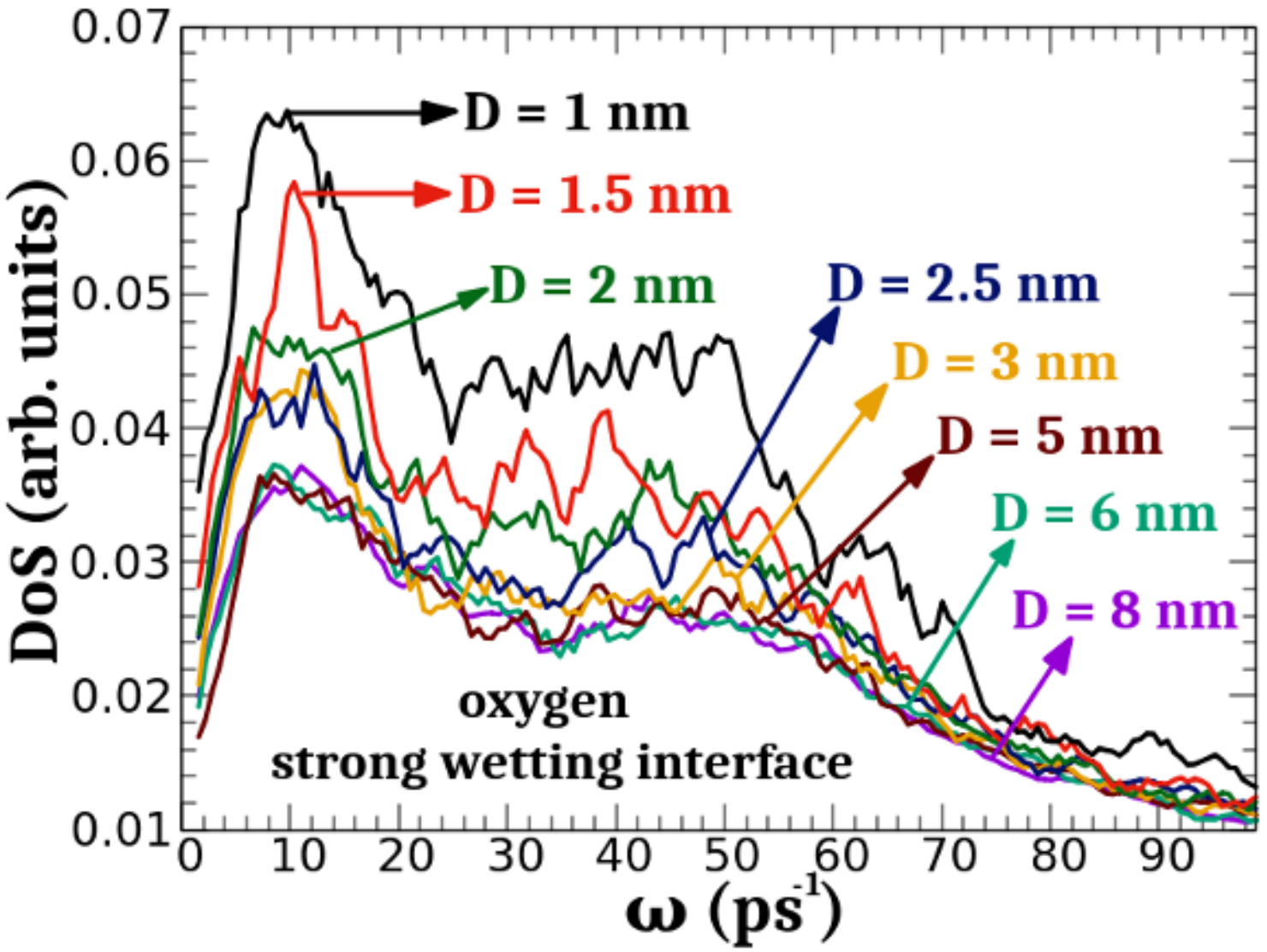
0.07
0.06
0.05
0.04
0.03
0.02
0.01
DoS (arb. units)
0
10
20
30
40
50
60
70
80
90
ω (ps-1)
D = 1 nm
D = 1.5 nm
D = 2 nm
D = 2.5 nm
D = 3 nm
D = 5 nm
D = 6 nm
D = 8 nm
oxygen
strong wetting interface

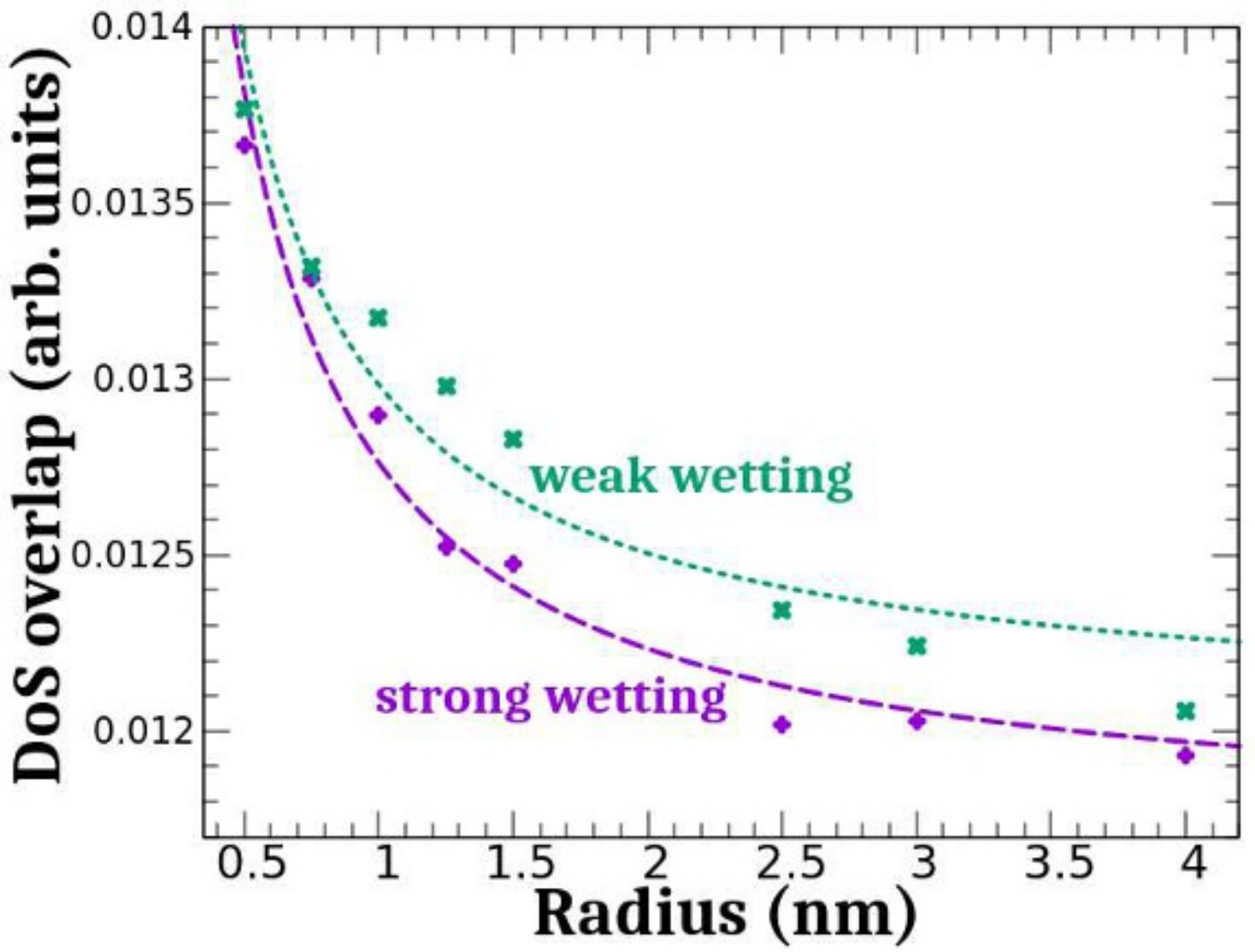
DoS overlap (arb. units)
0.014
0.0135
0.013
0.0125
0.012
weak wetting
strong wetting
0.5
1
1.5
2
2.5
3
3.5
4
Radius (nm)

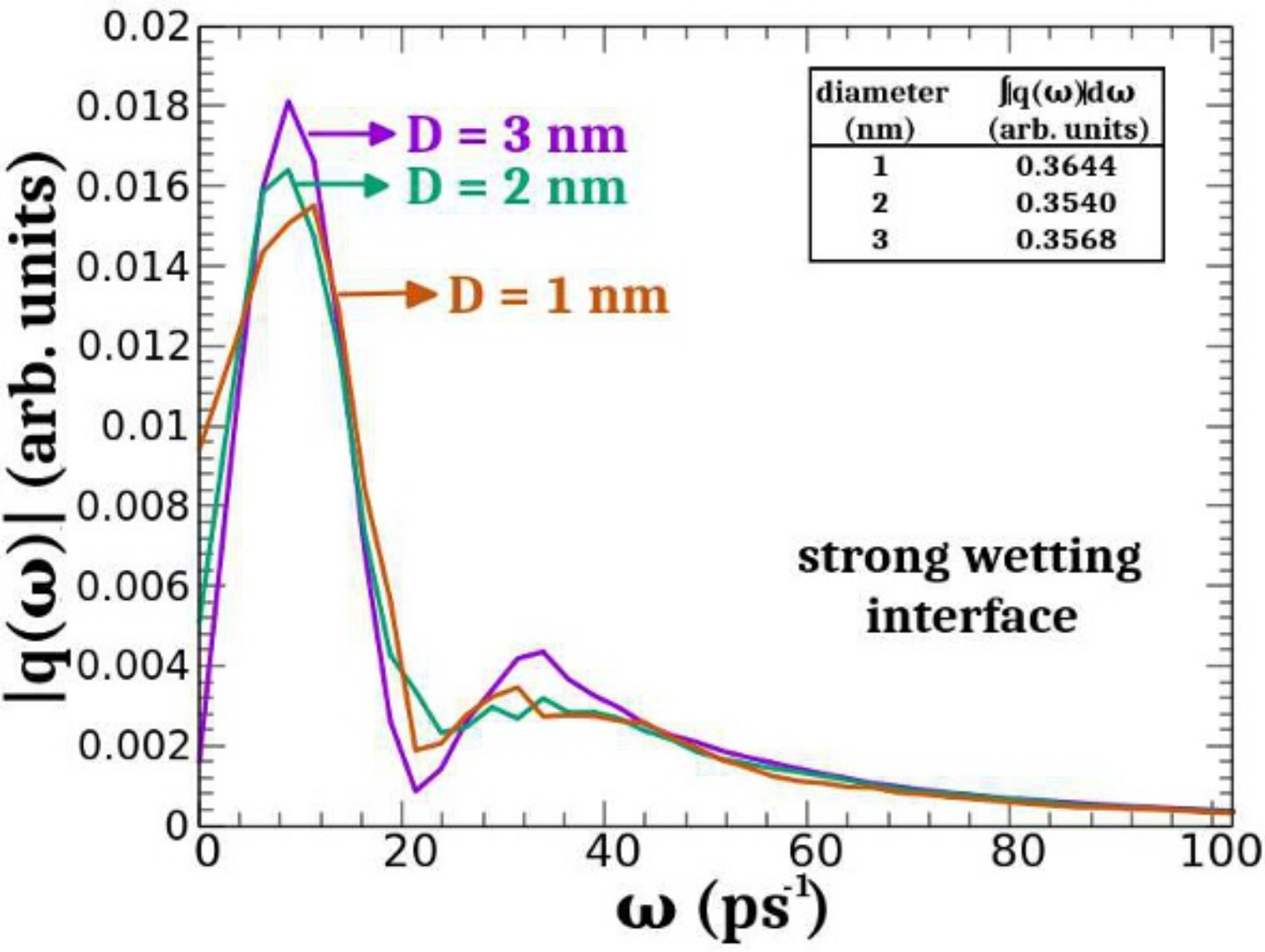
D = 3 nm
D = 2 nm
D = 1 nm
diameter (nm)
∫|q(ω)|dω (arb. units)
1
0.3644
2
0.3540
3
0.3568
strong wetting interface
|q(ω)| (arb. units)
ω (ps-1)
0
0.002
0.004
0.006
0.008
0.01
0.012
0.014
0.016
0.018
0.02
0
20
40
60
80
100

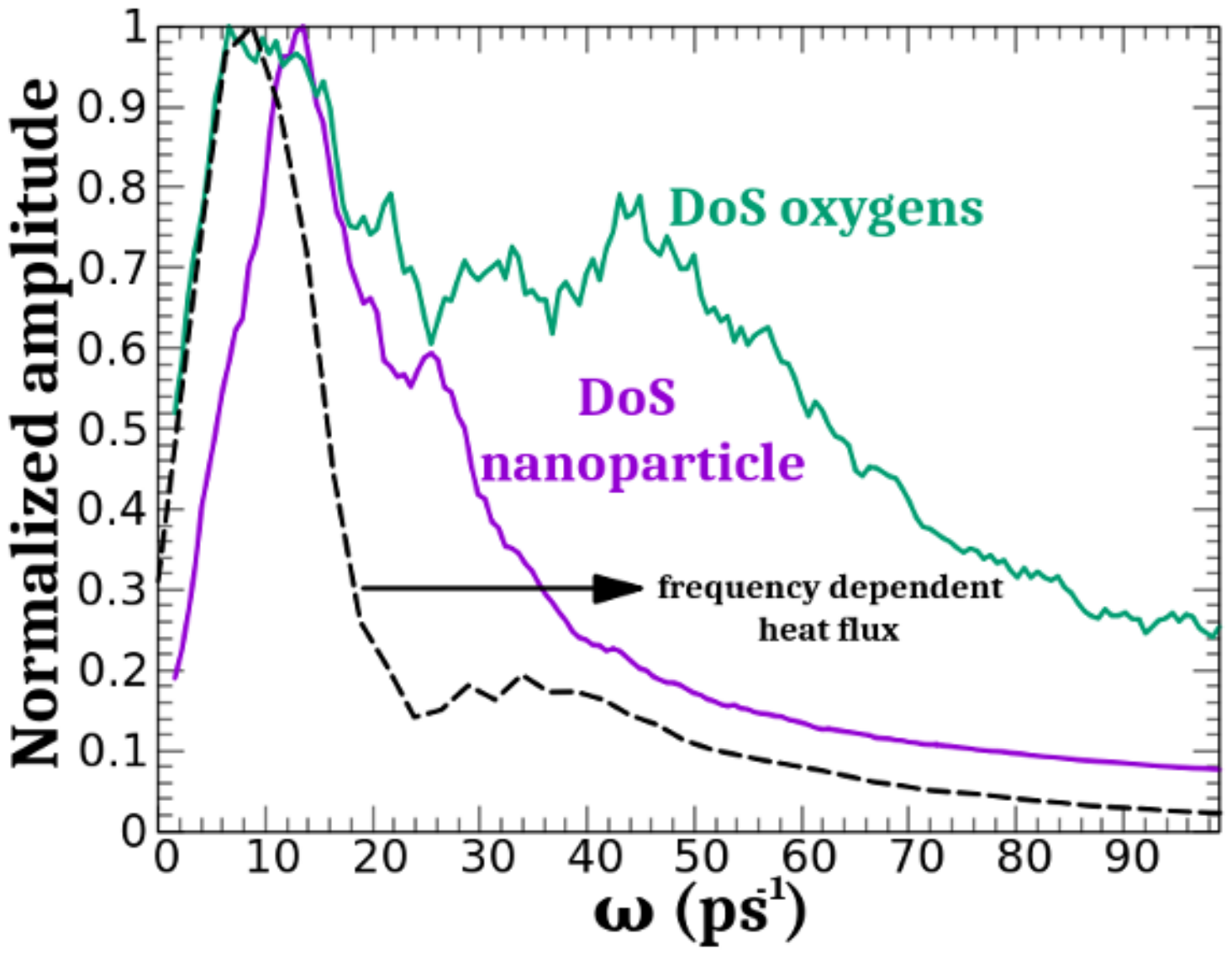
Normalized amplitude
1
0.9
0.8
0.7
0.6
0.5
0.4
0.3
0.2
0.1
0
0
10
20
30
40
50
60
70
80
90
ω (ps-1)
DoS oxygens
DoS
nanoparticle
frequency dependent
heat flux

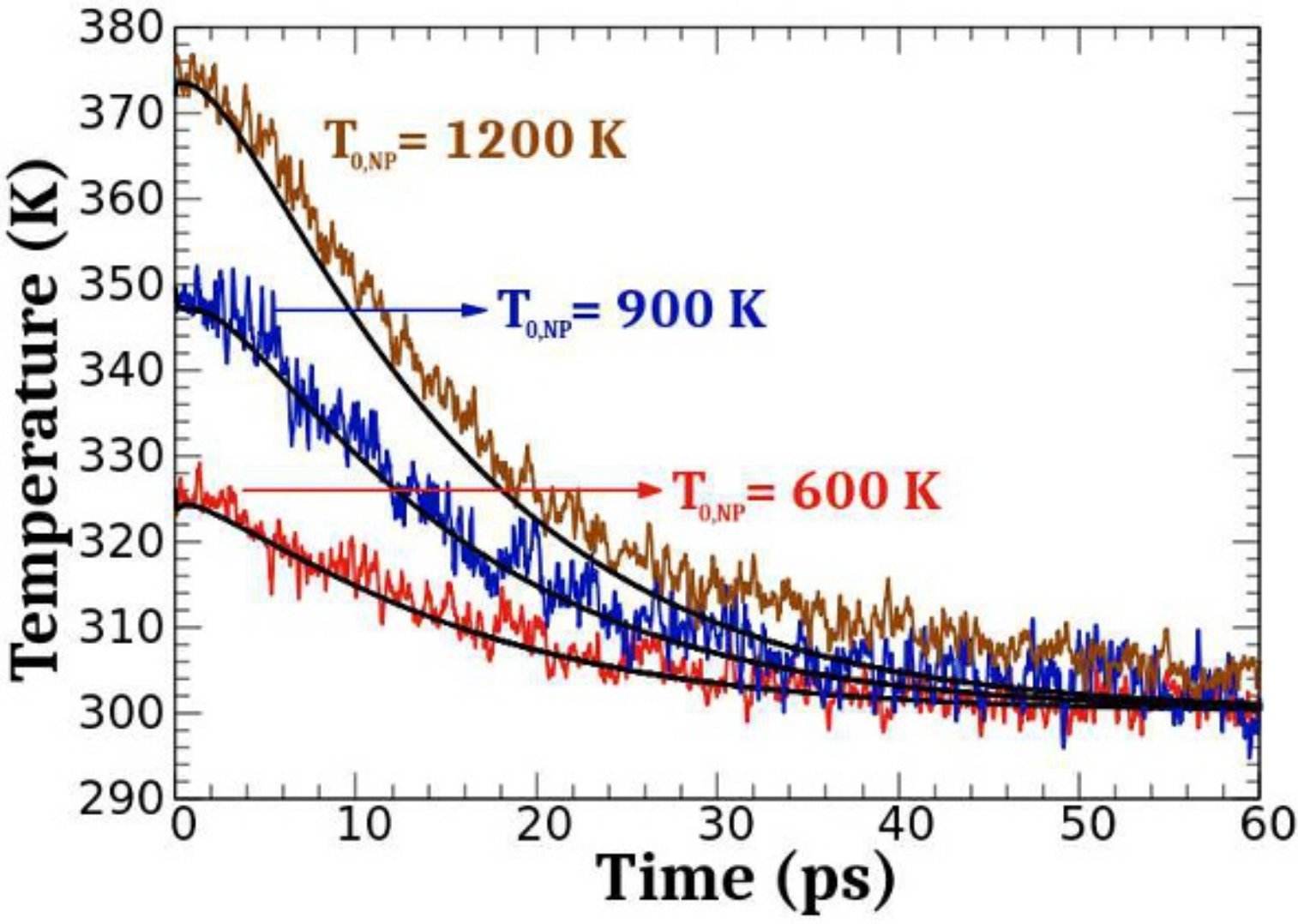
$T_{0,NP}$= 1200 K
$T_{0,NP}$= 900 K
$T_{0,NP}$= 600 K
Temperature (K)
Time (ps)
380
370
360
350
340
330
320
310
300
290
0
10
20
30
40
50
60

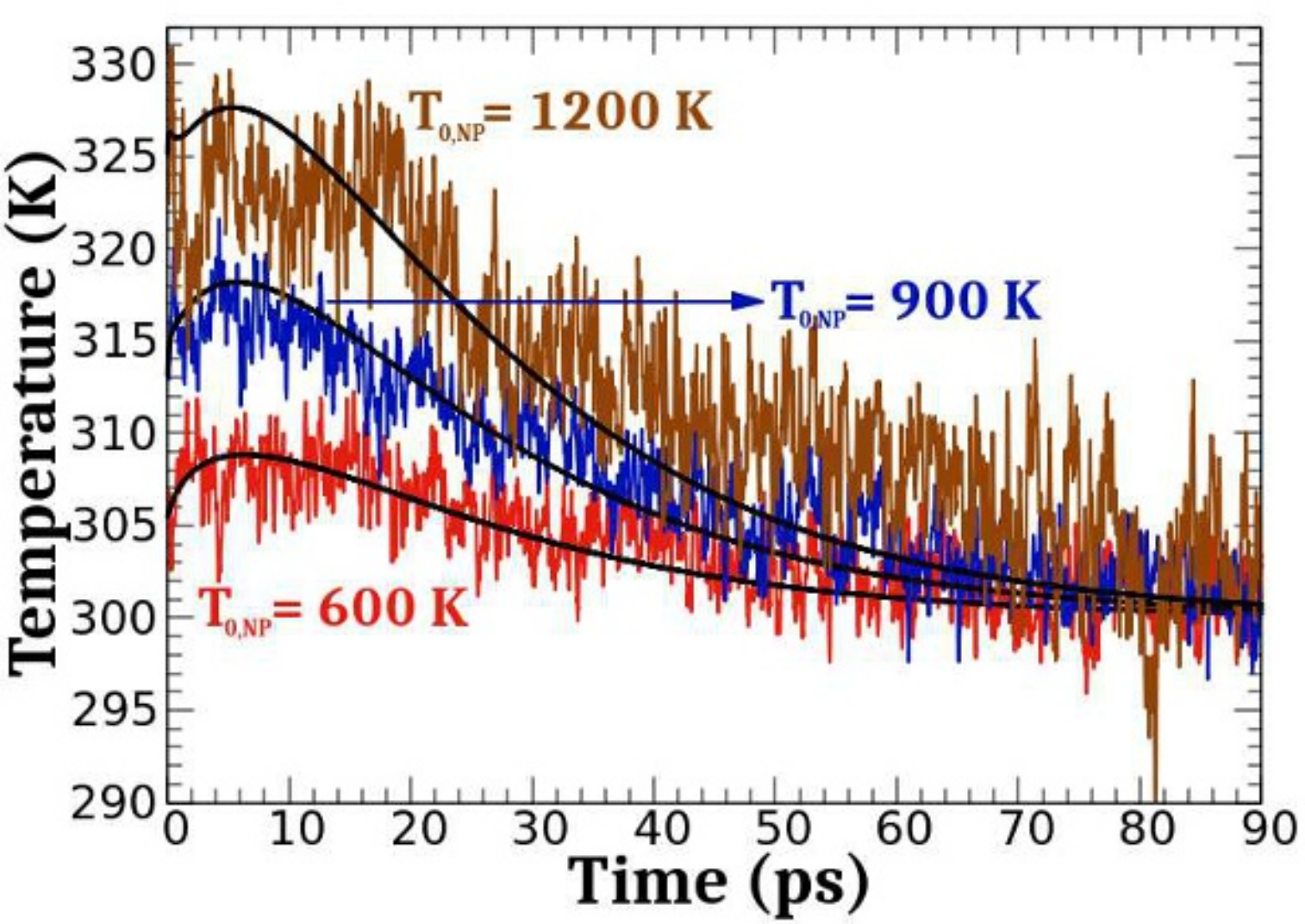
$T_{0,NP}$= 1200 K
$T_{0,NP}$= 900 K
$T_{0,NP}$= 600 K
Temperature (K)
Time (ps)
330
325
320
315
310
305
300
295
290
0
10
20
30
40
50
60
70
80
90

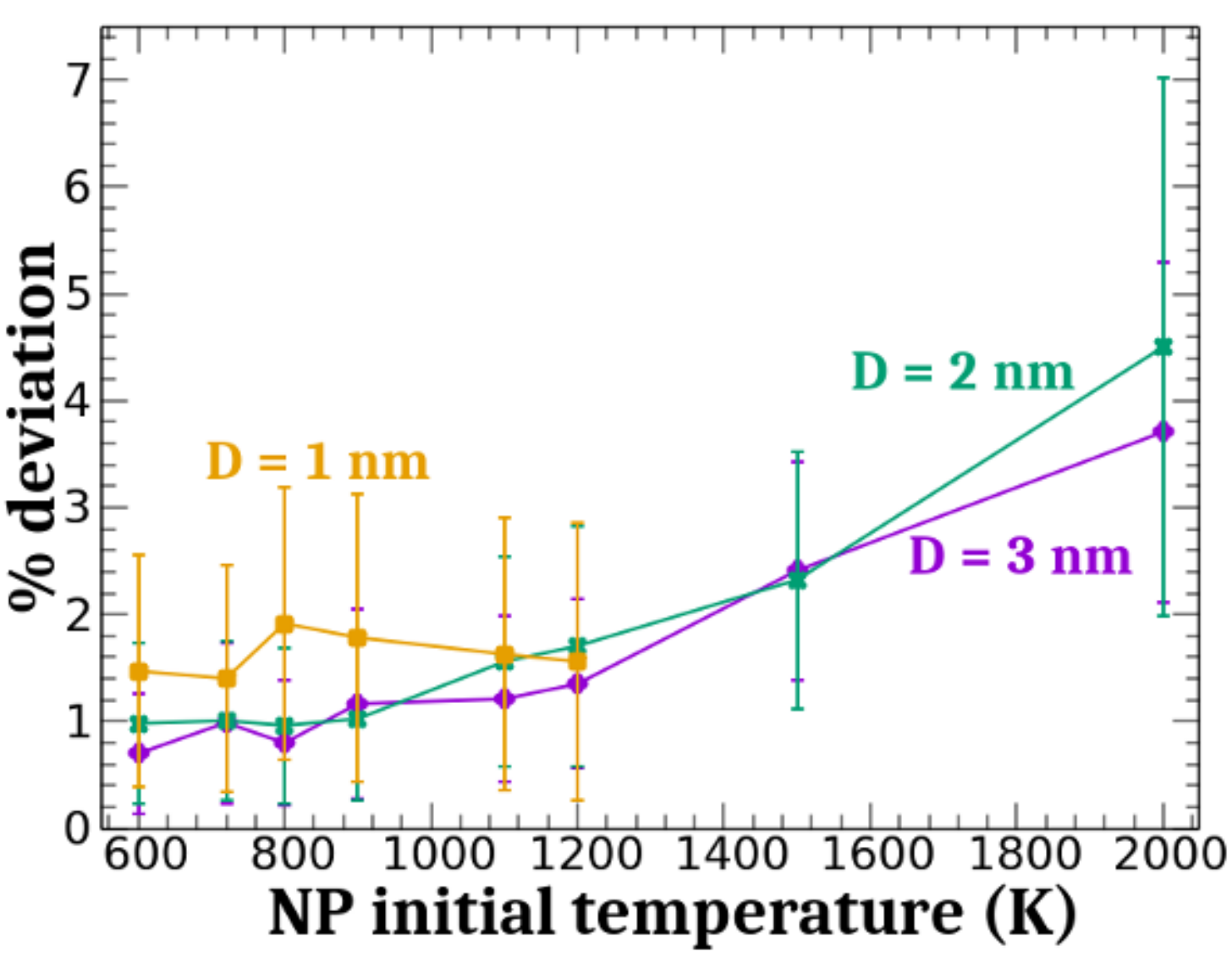
% deviation
NP initial temperature (K)
D = 1 nm
D = 2 nm
D = 3 nm
0
1
2
3
4
5
6
7
600
800
1000
1200
1400
1600
1800
2000